THE DETERMINATION OF MICROSTRAINS AND ANTIPHASE DOMAIN SIZE PRODUCED DURING ORDERING OF A Ni_4Mo SINGLE CRYSTAL

A THESIS

Presented to

The Faculty of the Division of Graduate

Studies and Research

by

Fu-Wen Ling

In Partial Fulfillment

of the Requirements for the Degree

Doctor of Philosophy in the School

of Chemical Engineering

Georgia Institute of Technology

December, 1970

In presenting the dissertation as a partial fulfillment of the requirements for an advanced degree from the Georgia Institute of Technology, I agree that the Library of the Institute shall make it available for inspection and circulation in accordance with its regulations governing materials of this type. I agree that permission to copy from, or to publish from, this dissertation may be granted by the professor under whose direction it was written, or, in his absence, by the Dean of the Graduate Division when such copying or publication is solely for scholarly purposes and does not involve potential financial gain. It is understood that any copying from, or publication of, this dissertation which involves potential financial gain will not be allowed without written permission.

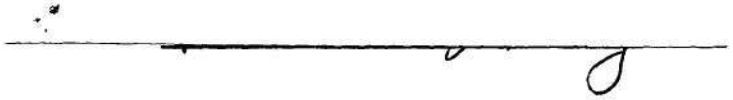

7/25/68

THE DETERMINATION OF MICROSTRAINS AND ANTIPHASE

DOMAIN SIZE PRODUCED DURING ORDERING OF A Ni_4Mo SINGLE CRYSTAL

Approved:

Chairman

Date Approved by Chairman: 11/23/70

ACKNOWLEDGEMENTS

The author wishes to express his sincere appreciation to his thesis advisor, Dr. E. A. Starke, Jr., for his helpful advice and continuous encouragement which were largely responsible for this work. The advice given by Dr. Stephen Spooner and Dr. R. J. Gerdes after reading the draft was most helpful. The useful suggestions of Dr. R. A. Young are also gratefully acknowledged.

The author is also grateful to the Department of Defense (Project THEMIS) and the United States Atomic Energy Commission, under contract number AT-(40-1)-3908, for their financial support of this study.

Last, but not least, the author wishes to thank his wife, Elena, for her patience and understanding during the period of this investigation.

TABLE OF CONTENTS

LIST OF FIGURES

Figure Page

LIST OF TABLE

SUMMARY

A single crystal of Ni_4Mo was studied by x-ray line broadening techniques using Warren's Fourier analysis employing computer methods. The long-range-order parameter, domain size and microstrains were measured after isothermal ageing at 700°C for various times.

The ordering occurs homogeneously inside the domains up to a long-range-order parameter of $S \simeq 0.7$. After $S \simeq 0.8$, further increase in the degree of order of the crystal is primarily by the elimination of domain boundaries due to domain growth. The rate of the domain growth is analogous to that of grain growth which follows the equation, $D^n - D_o^n = kt$. The magnitude of the parameter n is suggested to be dependent on the impurity content. The x-ray measured root-mean-square strain correlates directly with those calculated from the yield strength measurements. The high strength at the late stage of the ordering is mainly due to the high density of dislocations which are generated as a result of coherent interface strains.

CHAPTER I

INTRODUCTION

There are many solid solution alloys which develop a long-range-ordered structure at low temperatures. The ordering process involves a change from a random distribution of atoms among the lattice sites, to an arrangement having a larger unit cell where each atomic species prefers to be on particular lattice sites. The extent of long-range order is described by the parameter S which has been defined by Warren[1] as:

$$S = r_\alpha + r_\beta - 1 = r_\alpha - w_\beta = r_\beta - w_\alpha \qquad (1)$$

where

r_α = fraction of α-sites occupied by the right atom.

w_α = fraction of α-sites occupied by the wrong atom.

r_β = fraction of β-sites occupied by the right atom.

w_β = fraction of β-sites occupied by the wrong atom.

It is obvious that this parameter is unity when all sites are occupied by the correct atoms and zero when the distribution is random.

The ordering process involves atomic rearrangement by short-range diffusion. Provided that the initial and final structures contain the same chemical composition the kinetics might be expected to resemble those of an allotropic transformation. An order-disorder reaction may occur by two distinct mechanisms.[2] In one the formation of the superlattice is assumed to occur by a nucleation and growth process, beginning

at discrete centers, and continuing outwards until the disordered regions are consumed. The other mechanism involves a homogeneous process which proceeds simultaneously in all parts of the crystal. The nucleation mechanism involves an order-disorder interface and since there is usually a change in the lattice parameter of the two structures, there is lattice strain across the interface. However, the nuclei of a superlattice phase will tend to form homogeneously throughout the crystal, and the nucleation of the ordered phase at low temperatures in many ordering alloys is so easy that all parts of the material begin to transform at once and the nucleation and growth process approximates the homogeneous reaction.

Generally, if a change in density and crystal symmetry occurs during ordering, the reaction will tend to be of the nucleation and growth type. However, even under these circumstances the reaction will proceed more homogeneously as the temperature is lowered. In addition, impingement between the ordered domains usually occurs in a very short time and further increase in the degree of long-range order must be accomplished by interchange of the atoms within the domains. The kinetics during this state of ordering have been studied by Gorsky[3] and Vineyard[4] who applied various diffusion mechanisms to describe the process. They showed that the increase in the long-range-order parameter at a constant temperature is an exponential function of the time at that temperature.

There have been only a few studies of the kinetics of domain growth. Rudman[5] has suggested that the rate theory that is commonly applied to grain growth can also be applied to the growth of antiphase domains. This theory can usually be epxressed by the relation $D^n - D_o^n = kt$ where D_o is the initial domain diameter, D is the instantaneous domain diameter at

time t, k is a constant which depends on the diffusion coefficients, etc. and n is also a constant which in the original theoretical development was equal to two. Poquette and Mikkola[6] studied the rate of antiphase domain growth in Cu_3Au and found good agreement with the theoretical equation. They suggested that the value of n can be influenced by such complicating factors as the presence of impurities, the relative orientations of grains, and the effect of external surfaces on growing grains. The agreement of antiphase domain growth in Cu_3Au with grain growth kinetics is to be expected since impingement between the domains is completed at a very early stage and subsequent domain growth is due to the migration of the antiphase domain boundaries. It has not been established whether the grain growth theory can be applied to alloys such as Mg_3Cd in which the ordered nuclei are grown from the disordered matrix and to other alloys in which a high coherent boundary stress exists during the growth.

When an alloy undergoes an order-disorder transformation, it exhibits a marked change in both physical properties, such as electrical resistivity and magnetic susceptibility[7,8] and mechanical properties such as the elastic constants, yield strength, work hardening coefficient, and fracture behavior.[9] The changes in physical properties are usually attributed to a change in the electronic configuration of the atoms which accompany ordering, while the mechanical property changes have been attributed to numerous crystallographic features. The latter have been reviewed recently by Stoloff and Davies[9] and by Cahn.[10] Generally, the strengthening effect of order has been attributed to the degree of order, domain size and/or the strains produced during the ordering reaction,

although the details of the strengthening mechanisms are still unclear. Flinn[11] has suggested that the principal obstacle to slip in ordered alloys, at temperatures too low for rapid diffusion, is the presence of antiphase domain boundaries. Whenever a super-dislocation (i.e., a pair of dislocations which are total in the disordered lattice but partial in the ordered lattice) passes through an antiphase domain boundary, new boundary is formed requiring energy. Cottrell[12] has developed a theory which is applicable for small-domain-ordered alloys and relates the antiphase domain size to the yield strength. Kear[13] has attributed the steep work hardening rate on Cu_3Au to the pinning of super-dislocations by a cross slip mechanism, however, cross-slip in ordered alloys has been questioned by Cahn.[10]

Alloys which undergo a lattice distortion during ordering have the greatest potential for improving the strength during ordering.[14] The order transformation in these alloys is usually accompanied by large internal strains. There have been only a few studies of both ordering kinetics and mechanical properties of alloys which undergo a crystal structure change. These have been conducted on CuAu I[14,15,16] and Ni_4Mo.[17,18] However, quantitative determination of the most probable cause for strengthening in these alloys, e.g. the strains which accompany the order transformation, has not been attempted.

The present study was undertaken to quantitatively characterize the microstructural features, i.e., degree of order, antiphase domain size, and order strains, which influence the mechanical behavior of an ordered alloy. There are presently two experimental techniques which possess the resolution necessary for this characterization; transmission electron

microscopy and x-ray diffraction. Transmission electron microscopy has the advantage that the antiphase domain size and shape can be observed directly, but a quantitative determination of the degree of order and the microstrains accompanying the ordering process cannot be done. All of these parameters can be determined by x-ray diffraction techniques.[1]

Of the many alloys which might be chosen for a study of this nature, Ni_4Mo offers many advantages. Previous work has shown this material to exhibit a significant increase in strength during isothermal annealing below the critical temperature.[18] Disordered Ni_4Mo is a fcc solid solution which exhibits short-range order. Below about 868°C it transforms to an ordered body-centered tetragonal structure of the type $D1_8$. The bct unit cell is derived from the fcc cell by the transformation equations

$$\vec{a}_1' = \tfrac{1}{2}(3\vec{a}_1 + \vec{a}_2)$$

$$\vec{a}_2' = \tfrac{1}{2}(-\vec{a}_1 + 3\vec{a}_2)$$

$$\vec{c}' = \vec{a}_3$$

where $\vec{a}_1$, $\vec{a}_2$, $\vec{a}_3$ are the base vectors of the fcc lattice and $\vec{a}_1'$, $\vec{a}_2'$, $\vec{c}'$ are the base vectors of the bct superlattice. There is a slight contraction along the c' direction during ordering and the c'/a' of the tetragonal lattice is $0.986\ \sqrt{2/5}$. The orientation relationship of the ordered and disordered unit cells is shown in Figure 1. There are thirty possible ways for the ordered lattice to be nucleated from the disordered lattice since the c-axis of the tetragonal cell can be in any of the three original cubic axes; the rotational angle arctan (1/3) can be positive or negative;

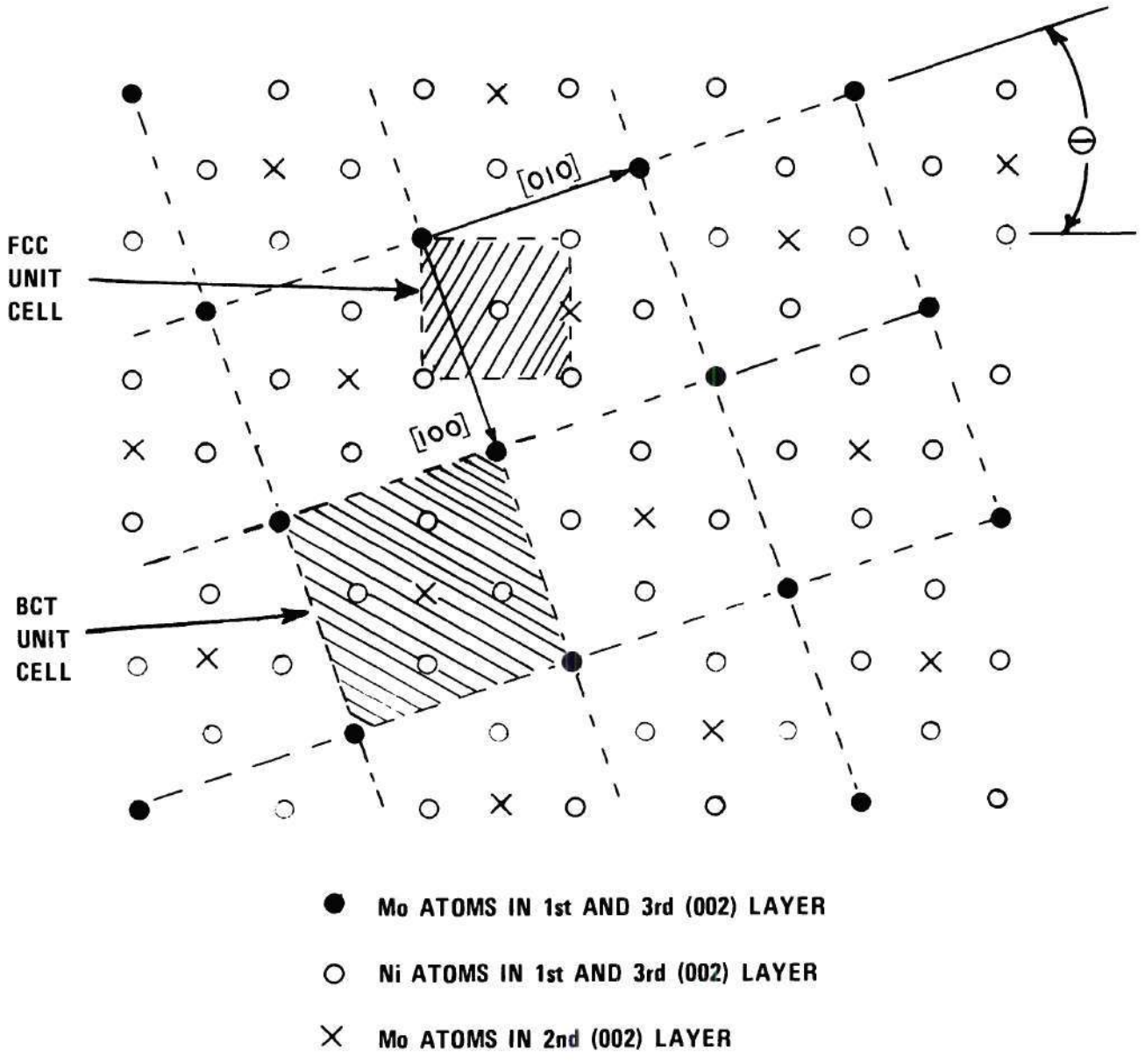

Figure 1. Schematic View of the Crystal Structure of Ni_4Mo, Viewing the Atomic Packing in (002) Planes. The 1st and 3rd Layers Coincide Exactly. Ni Atoms in the 2nd Layer are Not Shown.

and the origin of the unit cell can be at any of the five lattice sites. However, there are only six distinctly different orientations among the nuclei.

When the ordering process starts, the nuclei may originate from an arbitrary lattice site. Impingement of domains growing from different nuclei may create domain boundaries. When two domains with the same orientation (parallel c-axes, and same sign rotation angle) impinge, they may or may not have a domain boundary between them depending on the relative position of the unit cell origin of the nuclei. If a domain boundary is formed it will be an antiphase-domain boundary (APDB). When two domains with orthogonal c-axes impinge, a perpendicular-twin boundary (PTB) is formed. In general, the APDB has the lowest energy of the three since there is no appreciable distortion in this boundary except when a Mo-Mo relationship exists across the boundary. The APTB usually contains small strains due to the irregular distribution of Mo atoms in the boundary. The PTB has the highest energy of all three since the orthogonality of the c-axes of the domains creating the boundaries causes large distortions in the boundaries.

Ruedl et al.[17] have suggested that APTB and PTB will prefer to be $\{110\}_c$ planes since the domains forming these boundaries will be mirror images across this plane. However, due to the irregularity in domain shape, in general all APTB and PTB will not be $\{110\}_c$ planes. This will result in some boundaries having a larger lattice misfit than others.

In addition to the internal stresses in the vicinity of the various interfaces (APDB, APTB, PTB) there will also be bulk stresses produced by the ordering reaction. These are accommodation stresses resulting from

the c-axis contraction.

The ordering kinetics of Ni_4Mo are considerably influenced by the ordering temperature. Saburi et al.[19] using electron microscopic techniques, showed that ordering occurred by nucleation and growth at 800°C. The partially ordered nuclei were observable after five minutes at this temperature and impingement occurred after 30 minutes. At the lower temperature of 650°C no domains were observable after five minutes.[20] However, Okamoto[21] has recently observed very diffuse satellites in electron diffraction patterns of alloys quenched from above the critical temperature. This suggests that some form of ordered domain structure exists in the disordered alloy. On annealing at 750°C Okamoto found that impingement had occurred after about ten seconds. Consequently, the ordering reaction can be considered as essentially homogeneous at this and lower temperatures. After impingement a high strain contrast is observed in electron micrographs.[18]

The objective of the present study is to quantitatively characterize the structural features during progressive ordering of Ni_4Mo, an alloy which undergoes a lattice distortion during ordering, and to correlate these with the mechanical behavior. This study should lead to a better understanding of the order-disorder transformation and its effect on the mechanical behavior of alloys which undergo a crystal structure change during the ordering reaction.

CHAPTER II

EXPERIMENTAL METHODS

2.1. Sample Preparation

2.1a. Growth of Single Crystal: The single crystal of Ni_4Mo used in this study was kindly provided by Dr. J. E. Spruiell of the University of Tennessee. The crystal was grown using a modification of the Bridgman technique from a premelted alloy containing 20 atomic percent molybdenum, balance nickel. A detailed description of the experimental procedure used has been described elsewhere.[22]

2.1b. Crystal Orientation: A sample of 7/8 inch diameter and 3/16 inch thick was cut from the single crystal ingot. The initial surface of the crystal was cut parallel to the $(210)_C$ crystallographic plane. The sub-C designates the use of the cubic indices whereas sub-T will designate tetragonal indices. The $(210)_C$, $(531)_C$, and $(310)_C$ planes were chosen for line-broadening analysis since these planes correspond to the tetragonal indices of $(110)_T$, $(011)_T$, and $(200)_T$ respectively and have more than three orders available for study when using CuKα radiation. Since the normals to these planes are within 15° of one another, a single specimen could be prepared from the 7/8 inch diameter crystal with all three orientations and a surface area for each plane large enough for the diffractometer method of examination. It was necessary to have the diffraction surface parallel to the crystallographic plane so that the absorption correction could be eliminated.

The $(210)_C$ oriented sample was attached to goniometer head using a conductive adhesive and placed in the back reflection Laue camera. The sample was oriented so that the desired plane, $(531)_C$ or $(310)_C$, was perpendicular to the incident x-ray beam. The goniometer was then placed in a spark machine for planing. The orientation relationship between the planer and the x-ray machine was such that once the desired crystallographic plane was oriented perpendicular to the x-ray beam, the correct relationship was satisfied for planing this plane parallel to the surface of the crystal.

After the three planes were oriented and planed, the sample was removed from the goniometer head (by soaking in acetone) and the surface layer, which had been disturbed by spark machining, was removed by light hand grinding, mechanical polishing and chemical polishing. For chemical polishing a solution of 100cc H_2O, 225cc HNO_3, 150cc H_2SO_4, and 3 grams of NaCl was used at 90°C. The precision of the orientation of the desired surfaces prepared by this procedure were within 1°. A sketch of the sample is shown in Figure 2.

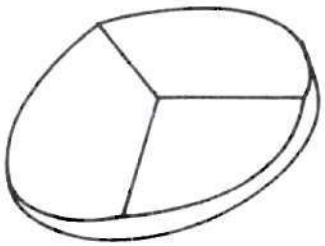

Figure 2. Sketch of the Sample

2.1c. Ordering Heat Treatment: The oriented single crystal was ordered to various degrees by isothermal ageing at 700°C. The temperature and ageing times were chosen from previous experience with Ni_4Mo polycrystalline samples.[18] All heat treatments were conducted under vacuum, and followed by ice-water quenching and chemical polishing. Before each ageing treatment the sample was cleaned with benzene to remove the wax used for attaching the sample to the x-ray goniometer head, soaked in acetone and rinsed with distilled water.

2.2. X-ray Measurements

The domain size and microstrains developed during progressive ordering at 700°C were measured by the x-ray line broadening method developed by Warren and Averbach.[1] The theory of the Warren-Averbach method is explained in Appendix A.

Fourier analysis of x-ray profiles has been derived with no restriction as to crystal structure. When applied to a superlattice, the root-mean-square (rms) strain can be obtained either by analyzing the superlattice reflections or the fundamental reflections. In addition to the dislocation strain field, the coherent domain boundary strain in an ordered material may also contribute to the measured rms strain. This is especially true in those alloys which undergo a crystal system change during the order-disorder transformation. The particle size obtained from superlattice reflections will be different from that obtained from fundamental reflections, since domain boundaries usually only affect the superlattice peaks.[6,23,24]

In Ni_4Mo the effect of twin boundaries (APTB, PTB) on the broadening of superlattice reflections is similar to the effect of grain and sub-grain

boundaries on fundamental reflections in pure metals. However, different antiphase domain boundaries may cause different broadening effects on different superlattice reflections. A quantitative analysis of these effects is complicated,[23] but the average particle size measured from superlattice reflections for various crystallographic directions can be considered as the average effective domain size.[6]

The x-ray measurements were made on a General Electric XRD-6 diffractometer and single-crystal orienter which was equipped with a Warren doubly-bent LiF monochrometer and automated in 2θ. A Cu target tube operating at 35KV and 1.2 to 17ma was used in conjunction with a proportional counter and single-channel analyzer. The procedure for aligning the equipment and the sample, for the data collection, are described in Appendix B.

The intensity distribution was measured for various reflections by automatic step scanning in 0.02° 2θ increments. The amount of data collected for a particular reflection depended on the breadth of the reflection as explained in Appendix C. The time for intensity accumulation was dependent on the intensity of the peak but was usually from 25 to 50 seconds. The $(110)_T$, $(220)_T$, $(330)_T$, $(440)_T$, $(200)_T$, $(400)_T$, $(600)_T$, $(011)_T$, $(022)_T$, and $(033)_T$ reflections were examined. The intensity profiles from these reflections were transformed into a Fourier series using computer techniques as described in Appendix C. The $(200)_C$ reflection from the disordered Ni_4Mo crystal was used for the instrumental correction employing the method of Stokes.[36] The Fourier coefficients were used to calculate the domain size and root-mean-square strains in the three different crystallographic directions.

As discussed in Appendix A, the integrated intensities of the superlattice reflections are proportional to the square of the long-range-order parameter, S, whereas the fundamental reflections are independent of the degree of order. The long-range-order parameter can, therefore, be calculated from a comparison of the integrated intensities of the superlattice and fundamental reflections using the relation

$$S^2 = \frac{E_i^s / R_i^s}{E_j^f / R_j^f} \quad , \tag{2}$$

where E_i^s and E_j^f are the measured intensities of the superlattice and fundamental reflections respectively and R_i^s and R_j^f are their corresponding calculated intensities. They are determined by,

$$R_i^s = v_i P_i F_i^2 (LP)_i \exp(-2M_i)$$

$$R_j^f = P_j F_j^2 (LP)_j \exp(-2M_j) \quad .$$

P is the multiplicity factor, and is one for a single crystal, F is the structure factor, LP the Lorentz-polarization factor, and exp (-2M) is the temperature factor. The value of v_i in the calculation represents the probability of having a particular orientation of the ordered domain. Since there are six unique ways in which the ordered lattice can develop with respect to the disordered lattice, this factor is 1/6 if all orientations have equal probability of forming.

During ordering the size and the distribution of the six differently oriented domains will become more and more irregular. The domains which

have their c-axis close to the sample surface normal will predominate in the late ordering stages since the contraction, which occurs along the c-axis, is more easily accommodated perpendicular than parallel to the surface. After one week at 700°C the $\{420\}_C$ fundamental reflection splits into three peaks. One of the peaks, which appeared at 144.10° 2θ, is attributed to domains which have their c-axis perpendicular to the surface normal and can be indexed as $(550)_T$ and $(710)_T$. The reflection which appears at 145.25° 2θ is attributed to $(262)_T$ and $(6\bar{2}2)_T$ planes from domains whose axis is 63.6° from the surface normal. The third reflection appears at 148.85° 2θ and is attributed to $(134)_T$ and $(3\bar{1}4)_T$ planes from domains whose c-axis is 26.4° from the sample surface normal. The volume fraction of these domains can be found from the ratio of their integrated intensities:

$$V_i : V_2 : V_3 = E_1/R_1 : E_2/R_2 : E_3/R_3$$

and

$$v_i = \tfrac{1}{2}V_i/(V_1 + V_2 + V_3)$$

Here we assume that the two different domains contributing to each reflection have the same probability of occurrance. After one week at 700°C, the volume percent of each is

$$V_1 : V_2 : V_3 = 0.3\% : 0.7\% : 99\%$$

and v_1 is equal to 0.15%. Assuming that there is equal probability of nucleating all six domain orientations and that the preferred orientation

comes during growth, the value of v_i for the calculation of R_i^s for different annealing times can be estimated from the domain size assuming a linear relationship. This was the procedure followed in calculating the long-range-order parameter, S, from the x-ray data.

Since the temperature factor for Ni_4Mo is unknown, the atomic scattering factors of Ni and Mo were corrected using the temperature factors of the pure metals similar to the procedure used elsewhere for Cu_3Au.[6,25] The error introduced by this procedure was minimized by using the $(440)_T$ superlattice and $(420)_C$ fundamental reflections for the calculation of S. These are the closest reflections along the same crystallographic direction.

CHAPTER III

RESULTS

The structural changes which accompany isothermal ageing of a previously disordered single crystal of Ni_4Mo below the critical temperature may be qualitatively described from x-ray traces. The gradual changes in the $(440)_T$ superlattice reflection and $(420)_C$ fundamental reflection are shown in Figure 3 which shows the traces after various ageing times at 700°C. During the ordering process the superlattice reflection becomes sharper and increases in intensity, whereas the fundamental reflection is broadened and the integrated intensity remains essentially constant. The behavior of the superlattice reflection is due to the increase in both the domain size and degree of order with ageing time. The broadening of the fundamental reflection is mainly attributed to the strains accompanying the ordering process.

After one week at 700°C the $(420)_C$ fundamental reflection split into three reflections corresponding to planes in domains with mutually perpendicular c-axes. The reflections which were indexed $(550)_T$, $(6\bar{2}2)_T$, and $(3\bar{1}4)_T$ could not be recorded in a single continuous 2θ scan because of their locations in reciprocal space. The orientation of the sample was adjusted by χ and Φ for each reflection so that the 2θ scan passed through the center of the reflection's reciprocal lattice point. The volume fraction of a particular domain was determined from the integrated intensity of the reflection from that domain as described in the

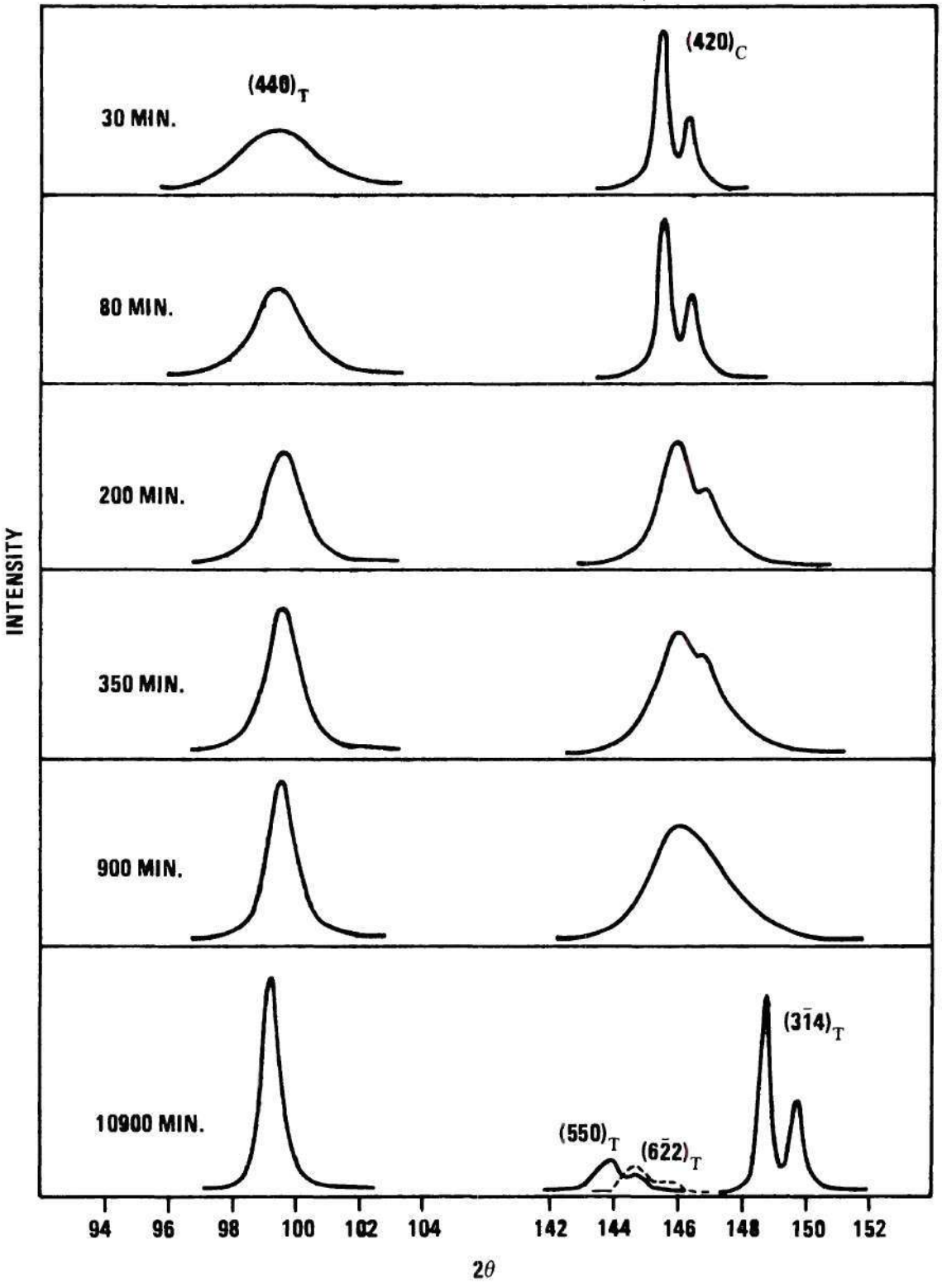

Figure 3. Change of the Peak Shape of a Superlattice and a Fundamental Reflection During Isothermal Ageing at 700°C. The Integrated Intensities of all the Reflections are Not Drawn to Scale.

preceding Chapter. The volume percent and the angles between the surface normal and the c-axes are as follows: 26.4°, 99 volume percent; 63.6°, 0.7 volume percent; 90°, 0.3 volume percent. This result indicates a predominance in the growth of domains whose c-axis is close to the surface normal. A schematic of the domain structure of ordered Ni_4Mo is given in Figure 4.

The long-range-order parameter was calculated from the integrated intensities of the $(440)_T$ and $(420)_C$ reflections after various ordering times at 700°C and are presented here in two ways. Figure 5 is a plot of ln(1-S) versus time and shows that the relation ln(1-S) = -kt is satisfied in the range S = 0 to S $\simeq$ 0.7. Figure 6 is a plot of ln S versus ln t and shows a linear relationship in the range S $\simeq$ 0.8 to S = 1.

The rms strain and antiphase domain size after various ordering times at 700°C were determined from line profile analysis as described in Appendix A and Chapter II. The computer techniques employed for the calculation of the Fourier coefficients from the raw data are described in Appendix C. The domain sizes thus determined for three crystallographic directions are plotted in Figure 7 as a function of ordering time at 700°C. Examination shows that the domains become more irregular and anisotropic with ageing time. However, the average size gives a linear relation in the ln D versus ln t plot with a slope of 2.9, Figure 8. In other words, the domain size satisfies the equation $D^{2.9} - D_o^{2.9} = k't$.

The rms strains for the three crystallographic directions and after various ageing times were plotted versus L as the example shown in Figure 9. Since the magnitude of the strain is dependent on L the value averaged from L = $0.1D_e$ to L = D_e were taken and denoted as $\langle \varepsilon^2 \rangle^{\frac{1}{2}}$. The

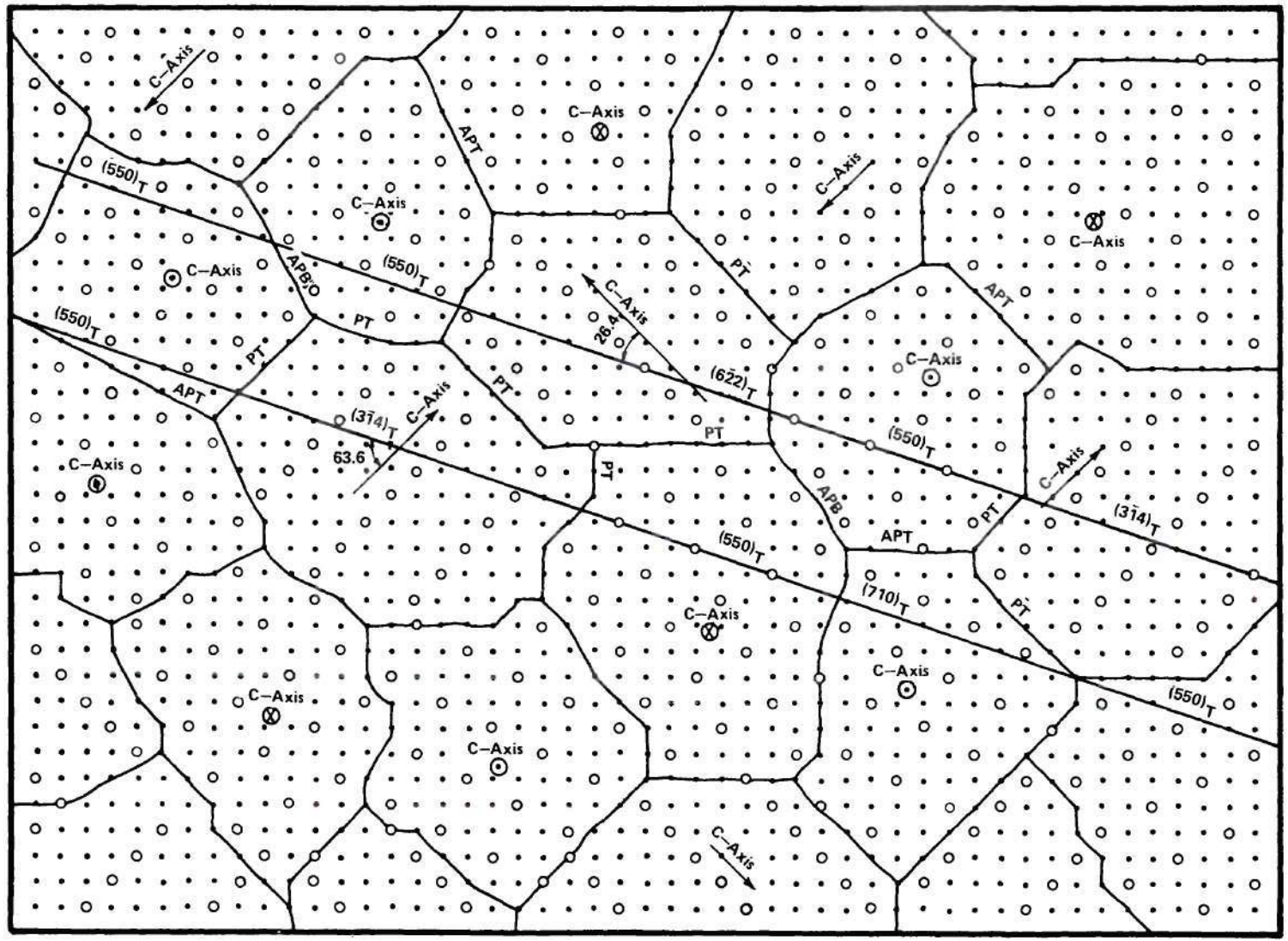

Figure 4. Schematic View of the Domain Structure on the $(0\bar{1}1)_C$ Plane. The Straight Lines are Parallel to the $(420)_C$ Planes.

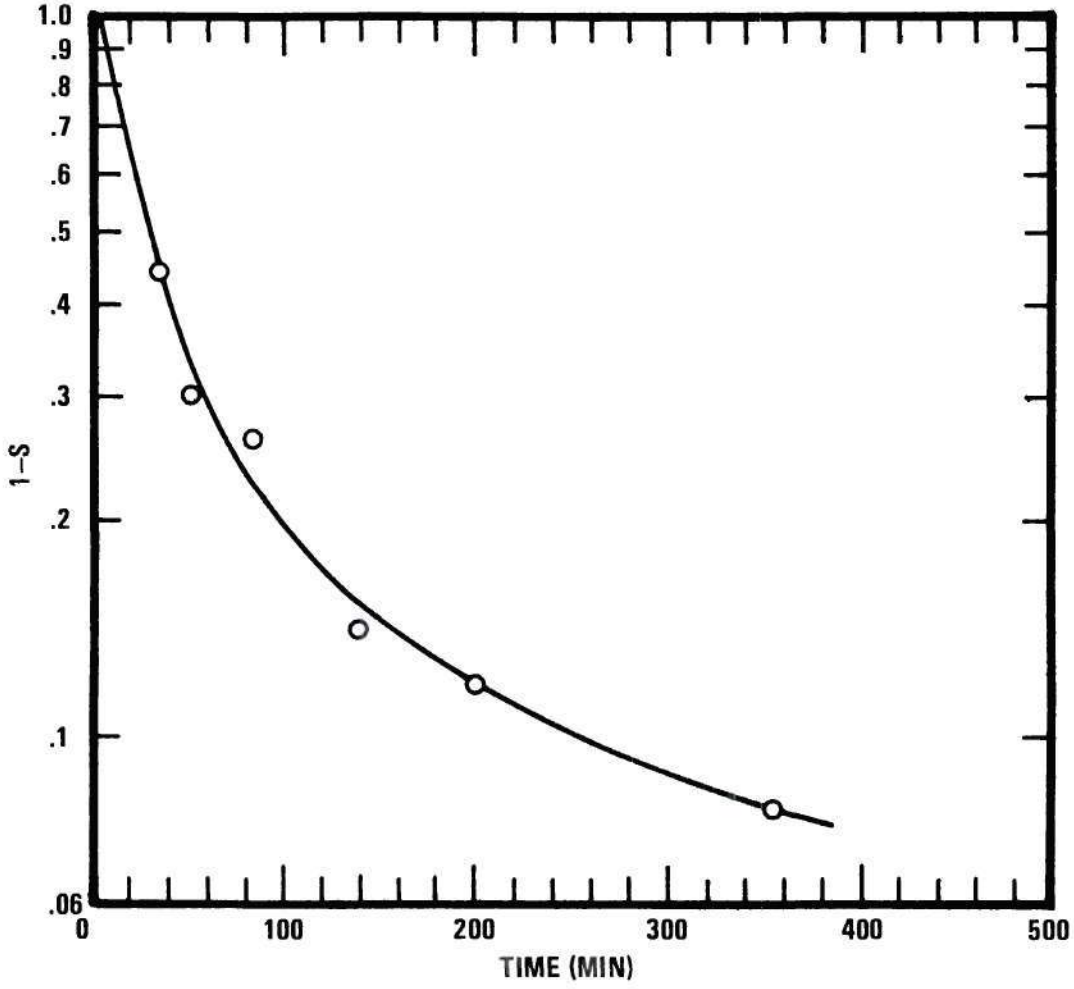

Figure 5. Ln(1-S) Versus Isothermal Ageing Time.

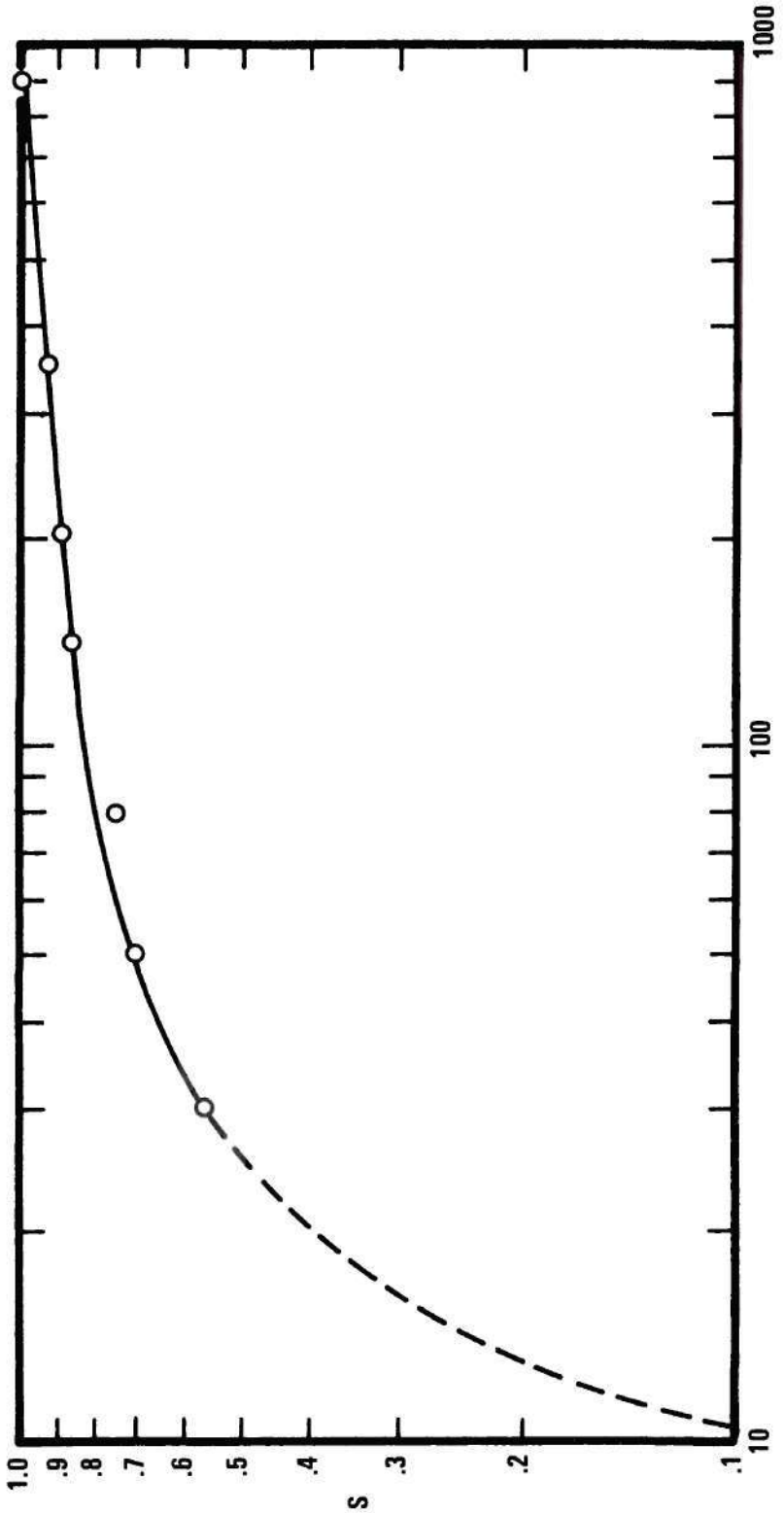

Figure 6. Ln-ln Plot of the Increase in the Long-Range-Order Parameter with Isothermal Ageing Time.

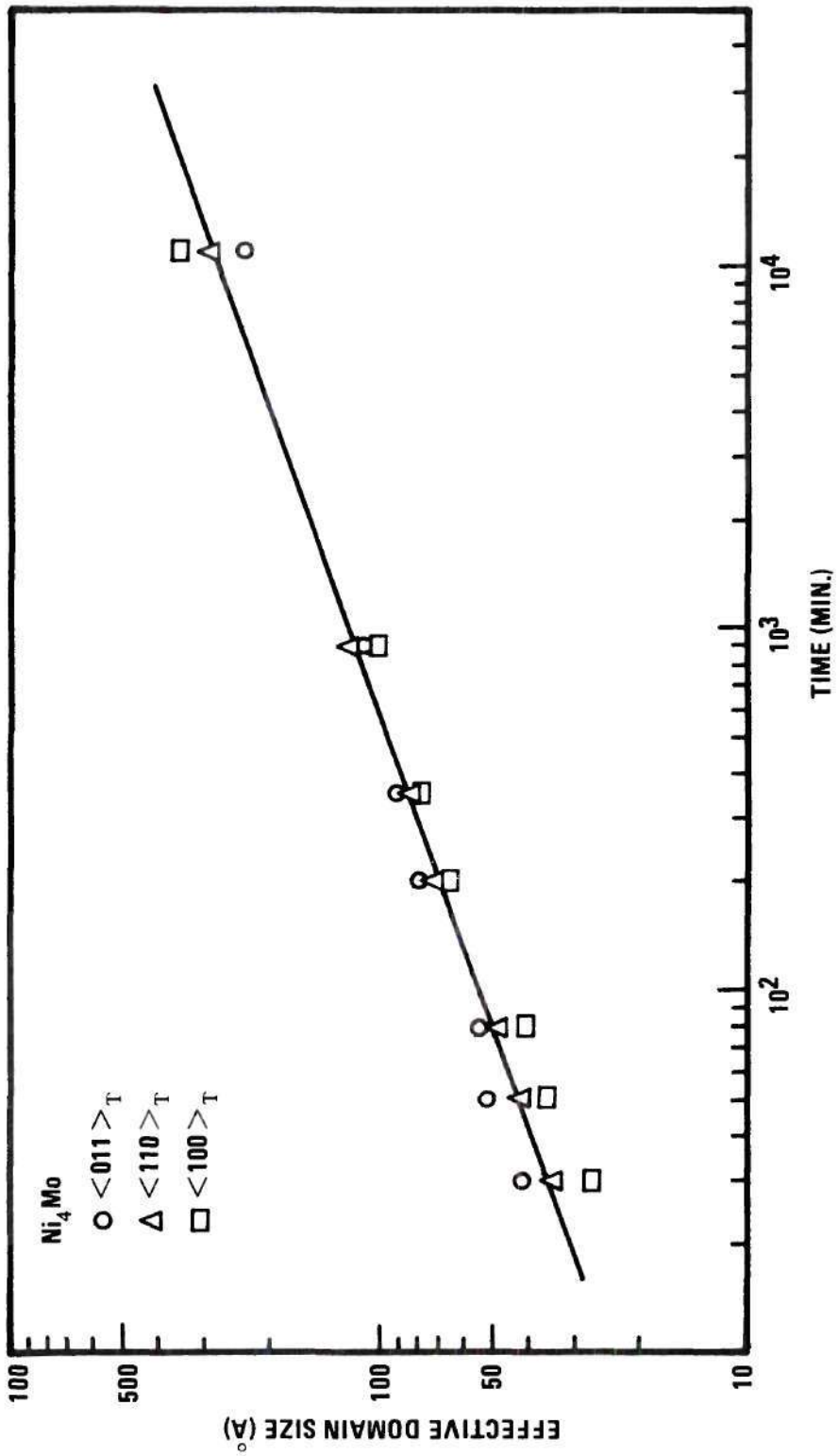

Figure 7. Ln Effective Domain Size Versus ln Ageing Time for Three Crystallographics Directions.

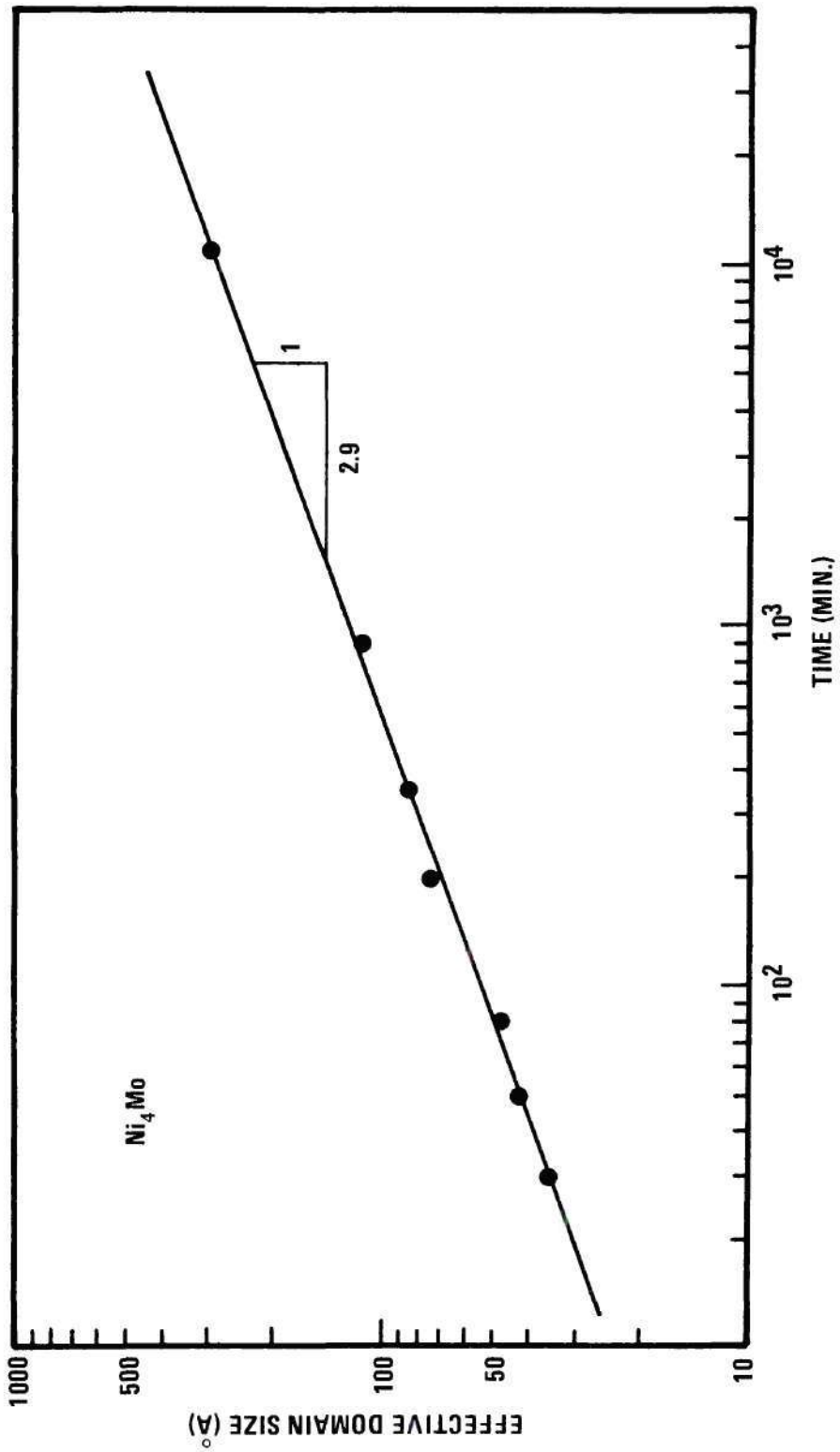

Figure 8. Ln Average Effective Domain Size Versus ln Ageing Time.

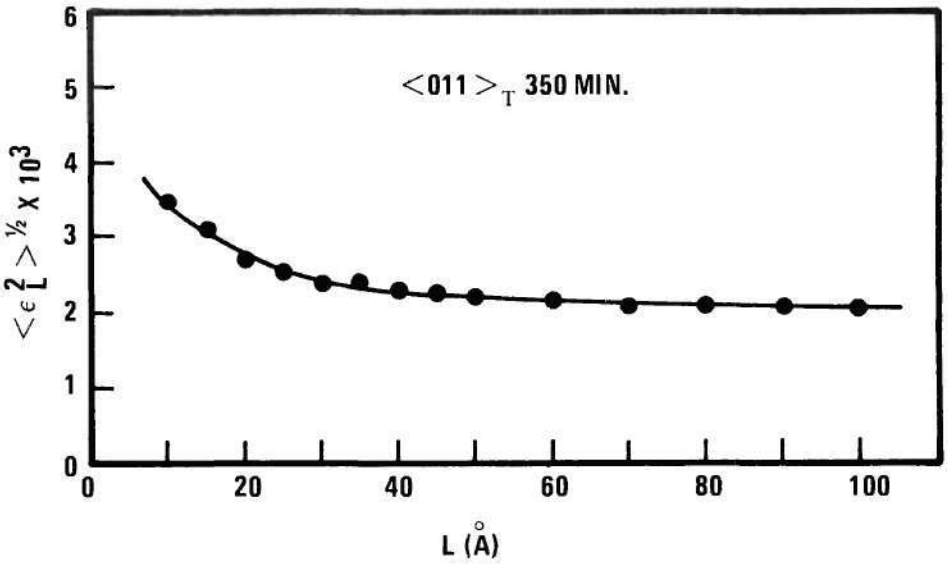

Figure 9. Root-Mean-Square Strain Versus L for the $(011)_T$ Direction After Ageing 350 Minutes at 700°C.

plot of the strains thus calculated versus average domain size $\langle D_e \rangle$, Figure 10, shows that the strain initially increases rapidly with domain size but after a certain size is obtained the internal strain remains essentially constant.

The long-range-order parameter, domain size and rms strain of Ni_4Mo ordered for various times at 700°C are listed, along with the yield strength measurements of Chakravarti et al.,[18] in Table 1.

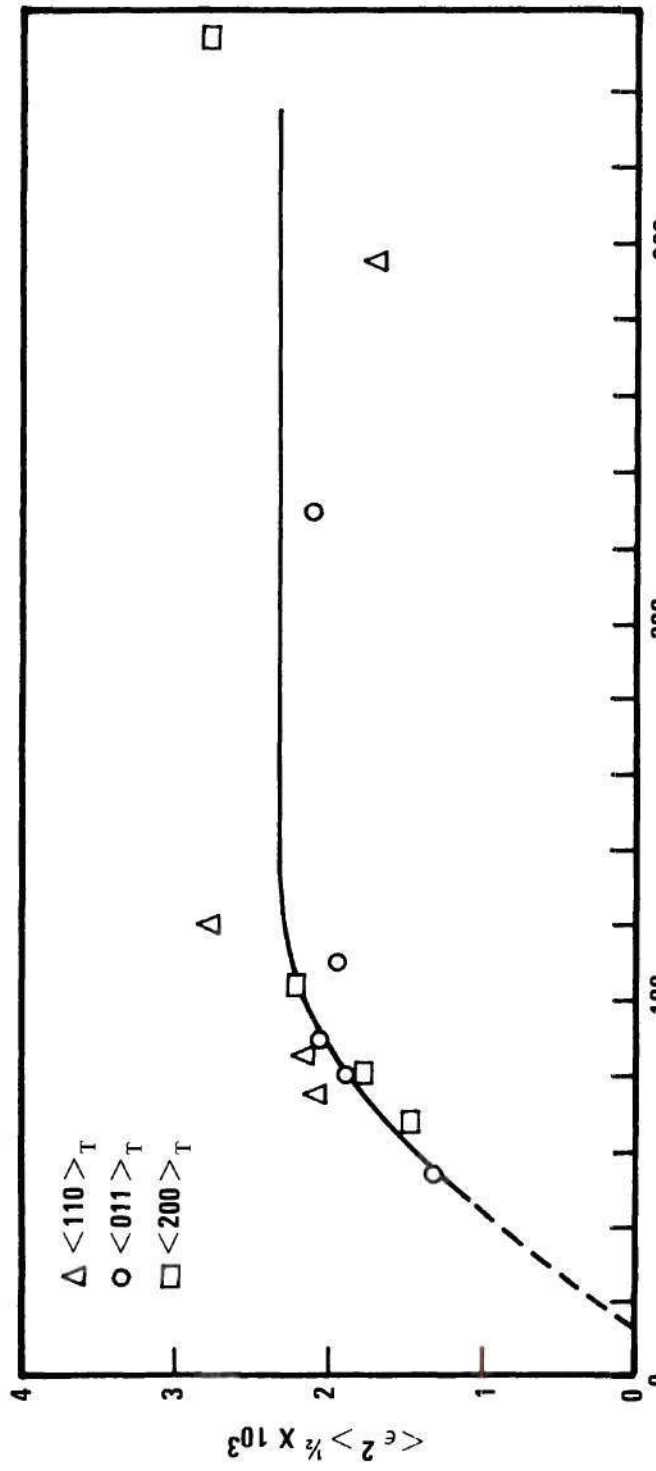

Figure 10. Root-Mean-Square Strain Versus Domain Size.

Table 1

The Long-range-order Parameter, Domain Size, rms Strain and Yield Stress After Various Ageing Times at 700°C

Ageing Time (min.)	Degree of Order (S)	Domain Size (Å)				rms Strain (10^{-3})				Yield Stress* (kg/cm^2)	$\Delta\sigma = \sigma_t - \sigma_o$ (kg/cm^2)	$\frac{\Delta\sigma_t}{E^{**}}$ (10^{-3})
		$(110)_T$	$(200)_T$	$(011)_T$	Average	$(110)_T$	$(200)_T$	$(011)_T$	Average			
0	0									3500	0	
30	.56	34	28	42	35	-	-	-				
(40)*	.64									6200	2700	1.3
50	.70	42	36	52	43	-	-	-				
80	.74	48	42	55	48	-	-	1.7				
(100)	.76									6720	3220	1.5
140	.86	-	-	-	-	-	-	-				
(180)	.81									7340	3840	1.8
200	.88	74	68	80	74	2.2	1.6	1.9	1.9			
350	.92	86	81	91	86	2.3	1.8	2.1	2.1			
900	.99	120	103	110	111	2.8	2.4	1.9	2.4			
(900)	1.00									7635	4135	2.0
10900	1.00	294	352	233	293	1.7	2.8	2.2	2.3			

*Yield Stress and S value at the ageing time with parenthesis are from Chakravorti et al.[18]

**$E = 2.11 \times 10^6$ kg/cm^2 after Chakravorti et al.[18]

CHAPTER IV

DISCUSSION OF RESULTS

4.1. Kinetics of Ordering

The gradual broadening, shifting and splitting of the fundamental reflections shown in Figure 3 is indicative of a homogeneous ordering process.[26] If the ordering reaction occurred by nucleation and growth of highly ordered domains from a disordered matrix, the three reflections which result from the splitting of the $(420)_C$ should be observed in the early stages of ordering. This is due to the fact that when the domains are highly ordered there is a marked difference in the d-spacing of the $(550)_T$, $(622)_T$ and $(314)_T$ planes. In some cases these reflections might not be resolved, but the broadening would increase drastically due to the overlap of the three peaks instead of gradually as observed.

Initially, the fundamental reflections were very sharp since the particle size was extremely large and there was an absence of internal strain. An analysis of the superlattice reflections gave a domain size of about 35Å after 30 minutes of ageing, and no measurable rms strain up to 50 minutes of ageing. With further ageing the fundamental reflections became broadened while the superlattice reflections sharpened. The sharpening of the superlattice reflections was due to the growth of the domains during ordering whereas the broadening of the fundamental reflections was due to the increase of rms strains.

After about one week of ageing the $(420)_C$ fundamental reflection splits into three different fundamental reflections, $(550)_T$, $(622)_T$, $(314)_T$.

These three reflections are from three different kinds of domains with differently oriented c-axes. The gradual shifting of the disordered peaks to positions corresponding to the tetragonal superlattice indicates the continuous contraction of the c-axis with increasing order. When the order is complete, the difference in Bragg angles of the three lines is maximized. However, even after an S of unity was obtained, the three reflections were not initially resolvable since the small domain size also caused a broadening. After one week, at 700°C the domain size was sufficient for resolution of the three peaks.

In homogeneous ordering, it is assumed that the transformation proceeds by short-range diffusion. The reaction occurs continuously and homogeneously throughout the crystal. Since ordering is accompanied by a decrease in free energy, a fictitious driving force, proportional to the fraction of atoms in the wrong lattice sites, may be assumed for this short-range diffusion. The probability of atoms "jumping" into the right sites will then be proportional to the fraction of atoms in the wrong sites. The possible "jump" mechanism may be through vacancies or by ring exchange. Neglecting the increase of order due to the diminution of the domain boundaries and assuming that whenever an atom "jumps" into the right site, it will stay, the rate of change of the long-range-order parameter may be written in the form,

$$\frac{dS(t)}{dt} = \frac{N(t)}{N_o} k(T) \qquad (3)$$

where N(t) is the total number of atoms in the wrong lattice sites at time t, and N_o is the value of N(t) at t = 0. k(T) is a parameter which depends on the diffusion coefficient of the elements and is a function of

temperature T. Using Warren's notation for the long-range-order parameter, we may write N(t) as

$$N(t) = [1 - r_{\alpha}(t)]N_o + [1 - r_{\beta}(t)]N_o \tag{4}$$

When t = 0, and assuming completely random disorder,

$$N(0) = (1 - X_A)N_o + (1 - X_B)N_o$$

$$= 2N_o - (X_A + X_B)N_o$$

$$= N_o$$

where X_A and X_B are the composition of the sample in atom fractions and $X_A + X_B = 1$. Simplifying equation (4)

$$N(t) = [2 - r_{\alpha}(t) - r_{\beta}(t)]N_o \tag{5}$$

By substituting equation (1) for the long-range-order parameter appearing in Chapter I, into (5)

$$N(t) = [1 - S(t)]N_o \tag{6}$$

Substituting equation (3) into (6)

$$\frac{dS(t)}{dt} = [1 - S(t)]k(T)$$

then

$$1 - S(t) = (1 - S_o) \exp(-kt) \tag{7}$$

where $S_o = S(0)$.

Equation (7) should be modified to include the equilibrium S since this value is not always unity. Denoting the equilibrium long-range-order parameter at the ageing temperature as S_∞, equation (7) becomes

$$S_\infty - S(t) = (S_\infty - S_o)\exp(-kt) \qquad (8)$$

Equation (8) is a general equation which describes the kinetics of ordering and is the same expression obtained by other authors [3,4] using a different approach.

The results of isothermal ageing Ni_4Mo at 700°C illustrated in Figure 5 show that in the region from S = 0 to S ≈ 0.7 the order reaction follows the equation

$$1 - S = \exp(-kt)$$

with k = 13.8 hr^{-1}. This supports the earlier conclusion that the ordering reaction is initially homogeneous. Since the partially ordered domains continue to grow after impingement, the long-range-order parameter of the crystal will increase by the reduction of the total domain boundary. However, the later effect should be small compared to that of ordering inside the domains when the long-range-order parameter of the crystal is low. This is especially true initially when the difference between the S value in the domain and that at the boundary is small.

When the long-range-order parameter of the crystal exceeds 0.7 the difference between the S value in the domain and that at the boundary will probably be large with the highest degree of order being inside the domain. In this late stage, ordering proceeds primarily by domain growth

since most of the disordered material is now in the domain boundaries. This conclusion is supported by comparing the plot of ln(S) versus ln(t) in Figure 6 with the plot of the logarithm of domain size versus ln(t) in Figure 8. A linear relationship is obtained for both the domain growth curve and the order parameter curve in the region from $S \simeq 0.8$ to $S = 1$. This is, at first consideration, unexpected since Warren[1] has shown that the antiphase domain boundary does not affect the integrated intensities of the fundamental and superlattice reflections. However, his result was derived from the assumption that the different atomic species always occupy the right sites in both domains up to the plane of atoms forming the boundary. This may be true when the domain boundary is created by dislocation motion during deformation. However, the assumption is probably incorrect for boundaries created by the impingement of two domains. A similar argument can be given for APTB's and PTB's.

In summary, the present results indicate that isothermal ordering of Ni_4Mo at 700°C proceeds primarily by the homogeneous process of short-range diffusion until an order parameter of $S \simeq 0.7$ is obtained. Here a gradual change occurs and after $S \simeq 0.8$ further improvement in the degree of order is produced primarily by domain growth and the resulting elimination of domain boundaries.

4.2. Domain Growth

The change in average domain size of Ni_4Mo with time at 700°C was shown in Figure 8 to follow the relationship developed for grain growth,[2,27,28] $D^n - D_o^n = kt$, with $n = 2.9$. A similar relationship with $n = 2$, has been found by English[29] for domain growth in Fe-Co-2V and by

Poquette and Mikkola[6] for domain growth in Cu_3Au. In addition, if the data on the domain size of Mg_3Cd measured by Davies and Stoloff[30] is replotted versus logarithm ageing time, Figure 11, the growth can also be described by $D^n - D_o^n = kt$, with $n = 3.3$. From the available data, therefore, it appears that domain growth in ordered alloys during isothermal ageing can be described by this size-time relationship.

The order transformations in the three systems, Fe-Co-2V, Cu_3Au and Mg_3Cd, unlike Ni_4Mo, do not undergo a crystal system change when going from the disordered to the ordered state. Therefore, the interface strain energy between the ordered and ordered or ordered and disordered regions is low when compared with that of Ni_4Mo. In Fe-Co-2V and Cu_3Au the impingement of the ordered domains occurs in the very early stage, and ordering proceeds homogeneously as in Ni_4Mo. On the other hand, the majority of the domain growth shown in Figure 11 for Mg_3Cd occurs before impingement of the ordered domains. The ordering process in Mg_3Cd is primarily heterogeneous. It would appear that domain growth in the three systems would occur by different mechanisms. It is striking that they all follow the same size-time relationship as that for incoherent grain boundaries.

The migration of grain boundaries has been attributed to the interface tension,[2] a concept which can also be applied to domain boundaries. However, the energy of grain boundaries is usually independent of boundary orientation (except for low angle subgrain boundaries) while the energy of domain boundaries depends on their orientation. The domain boundaries tend to lie in planes of low energy resulting in an irregular domain shape, e.g. "Swiss cheese"[29] while grains are usually polyhedral.

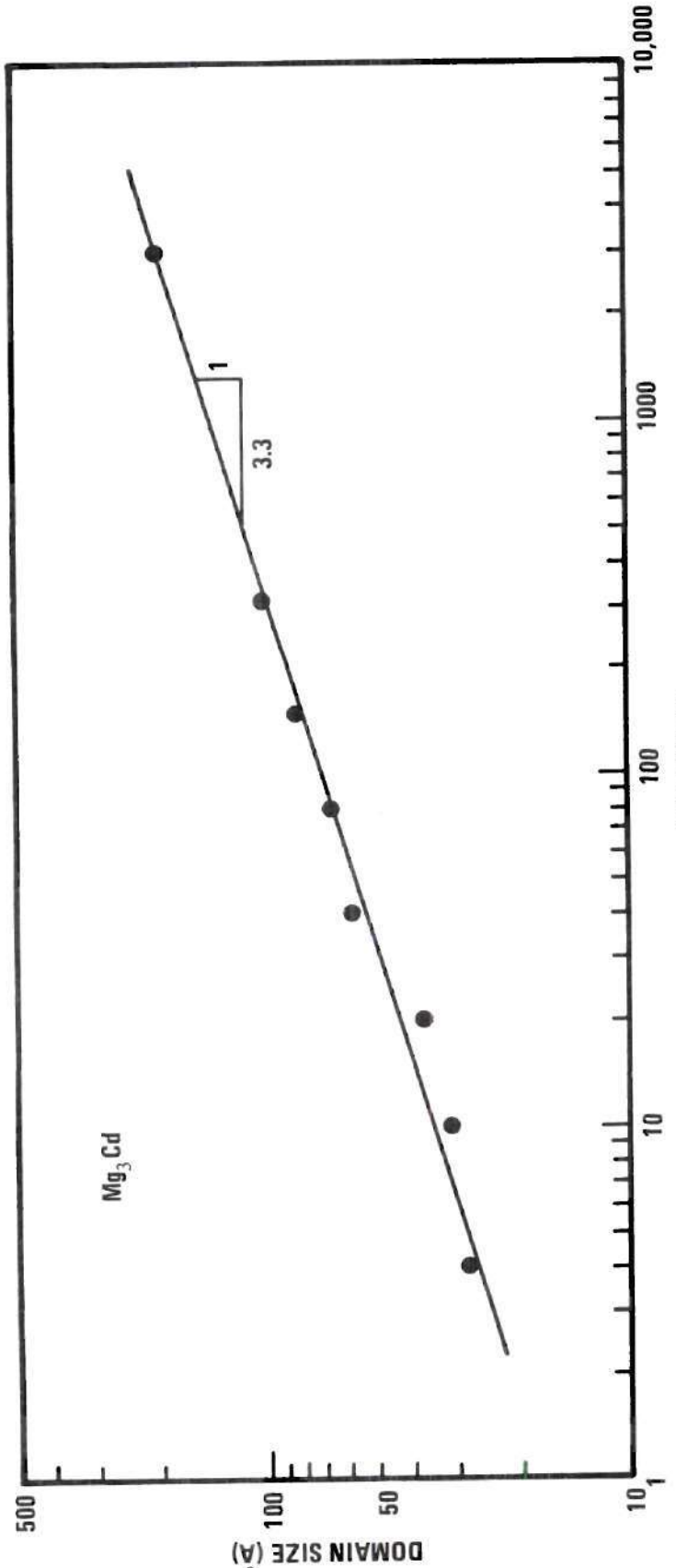

Figure 11. Ln Domain Size Versus ln Ageing Time for Mg_3Cd, Data from Davies and Stoloff.

In a recent study on zone-refined aluminum, Gordon and El-Bassyouni[31] found that the magnitude of n in the grain growth equation was mainly affected by impurity content with n decreasing with increasing purity. This qualitative correlation seems also to apply for domain growth in ordered alloys. The n obtained for Cu_3Au and Fe-Co-2V, alloys of high purity (~0.01 percent impurity) was considerably less than that obtained for Ni_4Mo and Mg_3Cd, alloys containing 0.13 percent and 0.3 percent impurities respectively.

During isothermal ageing of Ni_4Mo at 700°C the long-range-order parameter and rms strain increase continuously until an elapsed time of 900 minutes. Here, S has reached unity and the strain remains constant with further ageing. There is, however, no change in the average rate of domain growth. It appears that domain boundary migration is less influenced by strain and/or degree of order, than by other factors such as impurity content.

In summary, it appears that the domain growth in ordered alloys during isothermal ageing can be described by the grain-growth equation $D^n - D_o^n = kt$, and as for grain growth the value of n depends mainly on impurity content.

4.3. Order-Strengthening Mechanism

Figure 10 shows that the rms strain is mainly correlated with the long-range-order parameter but not with domain size because the microstrains do not increase with domain growth after the domain size reaches ~120Å. The long-range-order parameter reaches unity when the average domain size is about 120Å, see Figures 6 and 8.

The rms strain measured in three directions shows a significant increase with ageing time (Table 1). When the long-range-order parameter approaches unity after 900 minutes of ageing, the average rms strain reaches a maximum and then remains essentially constant. The hardness results of Chakravarti et al.[18] on polycrystalline samples also showed no significant change after about the same heat treatment. The hardness and rms strain developed during ageing of Ni_4Mo at 700°C can be correlated directly with the long-range-order parameter. The contraction in the c-axis gradually increases with the degree of order and the lattice misfit at the boundaries contribute to the microstrain. If the strain fields of the coherent boundaries are the only sources for the measured rms strain, the rms strain and hardness should decrease after S reaches unity since domain growth eliminates some of the boundary. However, no significant change was observed in the hardness and rms strain after 30 hours and one week ageing, respectively, even though the domain continued to grow.

Brown and Woolhouse[32] have suggested that when a lattice misfit in the range 0.013 to 0.077 occurs across a boundary, the stress produced by this misfit, in conjunction with thermal fluctuations, can generate dislocations from the interface leaving misfit dislocations at the interface. Since the maximum misfit in Ni_4Mo is 0.014, this process could also occur during ordering in this system. The new dislocations would be created simultaneously with the migration of domain boundaries and the strains produced by the dislocations might counteract the reduction in strain from the elimination of boundary during domain growth. This would explain why the rms strain remains essentially constant after some critical time. Using the maximum rms strain averaged over the three

crystallographic directions, a Burgers vector of $\frac{a_o}{2}\langle 110\rangle_C$ and equation (A.12) in Appendix A, the calculated dislocation density is $\sim 10^{11} cm^{-2}$. This is the same order of magnitude obtained from filings of pure metals.

It has been pointed out by many workers[33] that the rms strain obtained by x-ray analysis is of the order of the yield stress divided by Young's modulus. The value of Young's modulus for Ni_4Mo, $E = 2.11 \times 10^6$ kg/cm^2, and the yield stress for different annealing times at 700°C have been found previously.[18] If the values of $\Delta\sigma_{ys}$, the increase in yield stress from the disordered state after various ordering times, are divided by Young's modulus (Table 1), the results will mostly fall in the shaded region of Figure 12 which corresponds to the distribution of the rms strain obtained from x-ray measurements in three directions.

No measurable rms strain occurs in the three crystallographic directions up to 50 minutes. However, the tensile test for the polycrystal alloy aged for 40 minutes indicated a significant increase in yield stress, Table 1 and Figure 12. This may be considered as domain-size hardening or partial-order strengthening.[9] The domain size and long-range-order parameter for the alloy aged for 40 minutes are 37Å and 0.64 respectively. These are in the range for maximum domain-size strengthening and partial-order strengthening suggested for many alloys.[9]

The sources for the rms strain measured by x-ray techniques may be from the interface strain and/or from the dislocation strain field. Since the strained interfaces may act as dislocation sources, dislocations can be generated during ageing and the dislocation strain field will become more important with domain growth. The x-ray measured rms strain

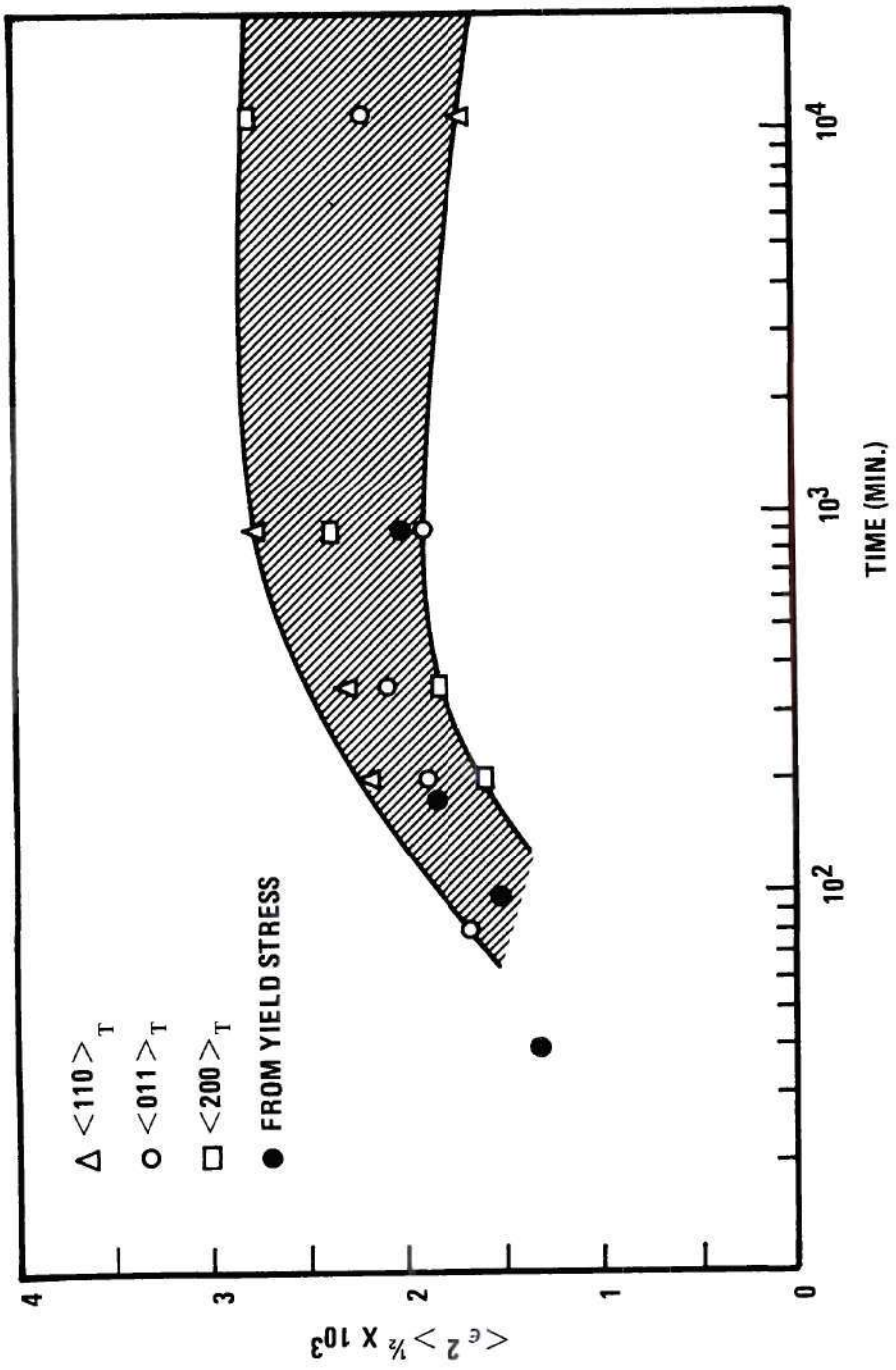

Figure 12. Root-Mean-Square Strain Versus Isothermal Ageing Time.

for the filings of nickel[34] is about 1.9×10^{-3}. For commercial nickel (99.4 percent Ni), the increase in the yield stress, from an annealed state to that of a cold worked state[35], divided by Young's modulus is also about 2×10^{-3}. These values are very close to the average rms strain measured in this study. This suggests that the microstrains induced by ordering Ni_4Mo, and thus the increase in strength, is analogous to that produced by the severe cold working of metals.

In summary, the x-ray measured rms strain agrees with that from the yield stress measurement. The order strengthening in the early stage is due to domain hardening and/or partial order. In the late stage, the interface strain and the dislocations, which are generated from the interface, strengthen the alloy.

CHAPTER V

CONCLUSIONS

1. The ordering of Ni_4Mo at 700°C proceeds homogeneously. Before the long-range-order parameter, S, reaches 0.7, the ordering primarily occurs inside the domains and follows the relation, $1 - S = \exp(-kt)$. After $S \simeq 0.8$, further increase in the long-range-order parameter of the crystal is accomplished by the reduction of domain boundaries and follows the relation, $\ln S = k' \ln(t/t_o)$.
2. The rate of domain growth during isothermal ageing is analogous to that of grain growth and follows the rate equation $D^n - D_o^n = kt$. The parameter n is mainly dependent on the impurity content.
3. The high strength in the late stage of ordering is mainly due to the high density of dislocations which are generated from the strained coherent interfaces.

APPENDIX A

THEORY OF X-RAY DIFFRACTION METHODS

Warren-Averbach Method

There are three major sources which cause the broadening and shifting of x-ray diffraction peaks. These are crystal distortion, small crystallite size and faulting. By representing the peak shapes as a Fourier series, Warren and Averbach have shown how these three effects can be separated. The following discussion will follow closely to that presented by Warren.[1]

In a distorted crystal the position of each unit cell is represented by the vector,

$$\vec{R}_m = m_1\vec{a}_1 + m_2\vec{a}_2 + m_3\vec{a}_3 + \vec{\delta}m \qquad (A.1)$$

where $\vec{a}_1$, $\vec{a}_2$ and $\vec{a}_3$ are the crystal axes and the displacement $\vec{\delta}_m$ allows for distortions within a domain, and is generally different for each cell identified by $m_1m_2m_3$, within the domain.

The displacement can be written,

$$\vec{\delta}_m = X_m\vec{a}_1 + Y_m\vec{a}_2 + Z_m\vec{a}_3 \qquad (A.2)$$

where X_m, Y_m and Z_m are very small numbers.

Assuming that the strains are continuous, any distortion within the unit cell can be neglected and the same structure factor F can be used for all cells. The intensity from one domain (or crystal) is then given by the double sum,

$$I = F^2 \sum_m \sum_{m'} \exp 2\pi i\left(\frac{\vec{S}-\vec{S}_o}{\lambda}\right) \cdot (\vec{R}_{m'} - \vec{R}_m) \qquad (A.3)$$

The usual representation of the diffraction vector in terms of the continuous variables $h_1 h_2 h_3$ and the reciprocal lattice vectors $\vec{b}_1$, $\vec{b}_2$ and $\vec{b}_3$ is

$$(\vec{S} - \vec{S}_o)/\lambda = h_1\vec{b}_1 + h_2\vec{b}_2 + h_3\vec{b}_3.$$

Using equation (A.3) and the powder pattern theorem[1], the power distribution in the h_3 direction for (00ℓ) planes is

$$P(h_3) = KN \sum_n \left[A_n\ (\ \ell)\ \cos\ 2\pi n h_3 + B_n\ (\ \ell)\ \sin\ 2\pi n h_3\right] \qquad (A.4)$$

where

$A_n = \frac{N_n}{N_3}\ \langle\ \cos\ 2\pi n\ell\ Z_n\ \rangle$, $\langle\ \cos\ 2\pi n\ell\ Z_n\ \rangle$ is an average over all such pairs of nth neighbors in the same column for the whole sample,

$B_n = \frac{N_n}{N_3}\ \langle\ \sin\ 2\pi n\ell\ Z_n\ \rangle$,

N_n = average number of n pairs per column,

N_3 = average number of cells per column,

$h_3 = (2a_3\ \sin\ \theta)/\lambda$,

θ = diffraction angle,

N = total number of cells in the sample,

K = a slowly varying function of θ proportional to

$F^2(1 + \cos^2 2\theta)/\sin^2\ \theta$ for a powder sample and

$F^2(1 + \cos^2 2\theta)\ \cos\ \theta$ for a single crystal sample,

F = structure factor,

n = harmonic number of the Fourier series equal to the number of orthorhombic cells separating two cells in a pair in one column.

If we transform the experimental peak profile into the Fourier series given in equation (A.4), information concerning the column length and strain may be obtained from the cosine coefficients. However, in addition to the small particle size and strain broadening, there are always instrumental broadening effects due to experimental conditions such as slit width, imperfect focusing and sample condition. The Fourier coefficients are calculated from the experimental intensity profile by Euler formulas

$$A_n = \int_{-\frac{1}{2}}^{\frac{1}{2}} P'(h_3) \cos 2\pi n h_3 dh_3 \qquad (A.5)$$

$$B_n = \int_{-\frac{1}{2}}^{\frac{1}{2}} P'(h_3) \sin 2\pi n h_3 dh_3 \ . \qquad (A.6)$$

Where $P'(h_3)$ is the experimental intensity profile in reciprocal space. Following the method of Stokes,[36] the instrumental corrected coefficients are given directly by the quotients of the two sets of coefficients

$$A_n + iB_n = \frac{(A_n + iB_n)\text{c.w.}}{(A_n + iB_n)\text{ann.}} \ . \qquad (A.7)$$

These corrected Fourier coefficients represent a particular reflection and carry only the information of the crystal as expressed in equation (A.4).

The cosine coefficient is the product of the two quantities N_n/N_3 and $\langle \cos 2\pi \ell Z_n \rangle$. Since N_n/N_3 is dependent on the column length, it is defined as the size coefficient represented by $A_n^s = N_n/N_3$. The other

quantity $\langle \cos 2\pi \ell Z_n \rangle$ depends upon the displacement of the cells in the column and will be denoted as a strain coefficient $A_n^{\epsilon}(\ell) = \langle \cos 2\pi \ell Z_n \rangle$. The cosine coefficients then become

$$A_n = A_n^s A_n^{\epsilon}$$

and
$$\ln A_n(\ell) = \ln A_n^s + \ln A_n^{\epsilon}(\ell) \qquad (A.8)$$

Separation of A_n^s and A_n^{ϵ} from A_n is possible when more than two orders of reflection are available since A_n^s is independent of the order whereas $A_n^{\epsilon}(\ell)$ is dependent on the order of reflection, ℓ. For small values of ℓZ_n the cosine can be expanded as

$$\ln \langle \cos 2\pi \ell Z_n \rangle = \ln (1 - 2\pi^2 \ell^2 \langle Z_n^2 \rangle) \simeq - 2\pi^2 \ell^2 \langle Z_n^2 \rangle .$$

Equation (A.8) then becomes

$$\ln A_n(\ell) = \ln A_n^s - 2\pi^2 \ell^2 \langle Z_n^2 \rangle . \qquad (A.9)$$

The distance $L = na_3$ is the undistorted distance along the columns of cells perpendicular to the reflecting planes, and $\Delta L = a_3 Z_n$ is the displacement of the cells separated by a distance L. The strain is then defined as $\epsilon_L = \Delta L/L = Z_n/n$.

Although the theory has been developed for an (00ℓ) reflection of an orthorhombic crystal it applies to any plane of any crystal structure by using a fictitious planar indices $(00\ell')$, where $\ell' = a_3'/d$ is an integer, d is the real spacing of the reflecting plane and a_3' is a fictitious lattice parameter. Equation (A.9) is then written as a function of d instead

of ℓ' in order to apply directly to all the planes of any crystal system;

$$\ln A_L\left(\frac{1}{d}\right) = \ln A_L^s - 2\pi^2 \frac{2L^2}{d^2} \langle \epsilon_L^2 \rangle \qquad (A.10)$$

When plotting the values of $\ln A_L\left(\frac{1}{d}\right)$ versus $1/d^2$ as indicated by Figure 13 and 14, the intercepts at $1/d^2 = 0$ give the values of the size coefficients A_L^s, and the slopes give $-2\pi^2 L^2 \langle \epsilon_L^2 \rangle$ from which the root-mean-square (rms) strain $\langle \epsilon_L^2 \rangle^{\frac{1}{2}}$ can be calculated for different values of L. To interpret the values of A_L^s, we follow the treatment of Bertaut.[37] The crystal is represented as columns of cells and p(i) is the fraction of columns of length i cells. The value of N_n can then be expressed in terms of p(i).

$$N_n = \sum_{i=|n|}^{\infty} (i - |n|)\, p(i)$$

The size Fourier coefficients now are given by

$$A_n^s = \frac{1}{N} \int_{i=|n|}^{\infty} (i - |n|)\, p(i)\, di$$

and

$$\left(\frac{dA_n^s}{dn}\right)_{n \to o} = -\frac{1}{N_3} \qquad (A.11)$$

The average column length perpendicular to the reflecting planes is $L = N_3 a_3'$. It can be directly obtained from the negative inverse slope of A_L^s versus L, i.e.

$$\langle D \rangle = -\frac{1}{\left(\frac{d\, A_L^s}{d\, L}\right)_{L \to o}}$$, see Figure 15.

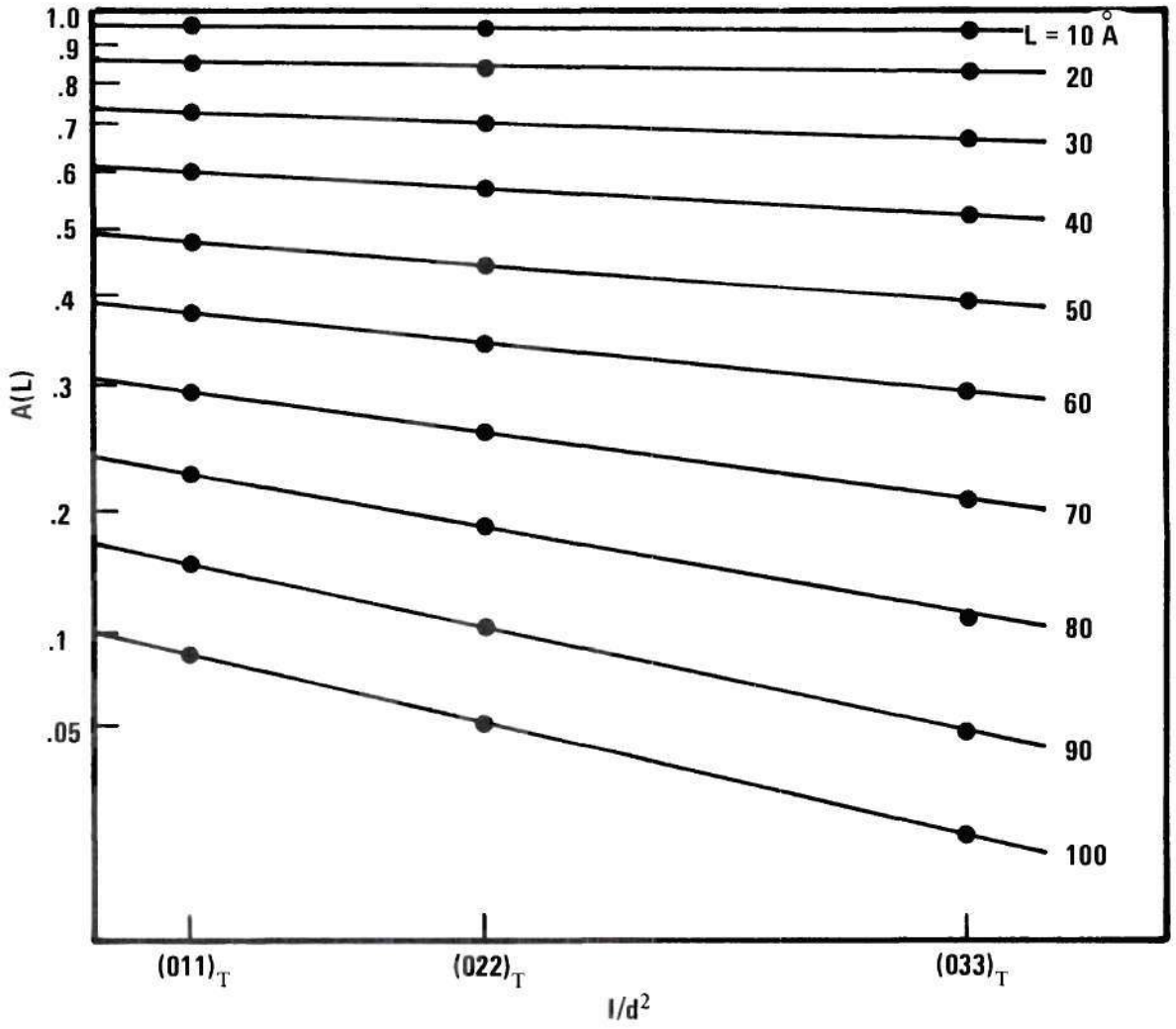

Figure 13. Fourier Coefficients of Various Orders of Reflection of a $(011)_T$ Plane for Different L Values.

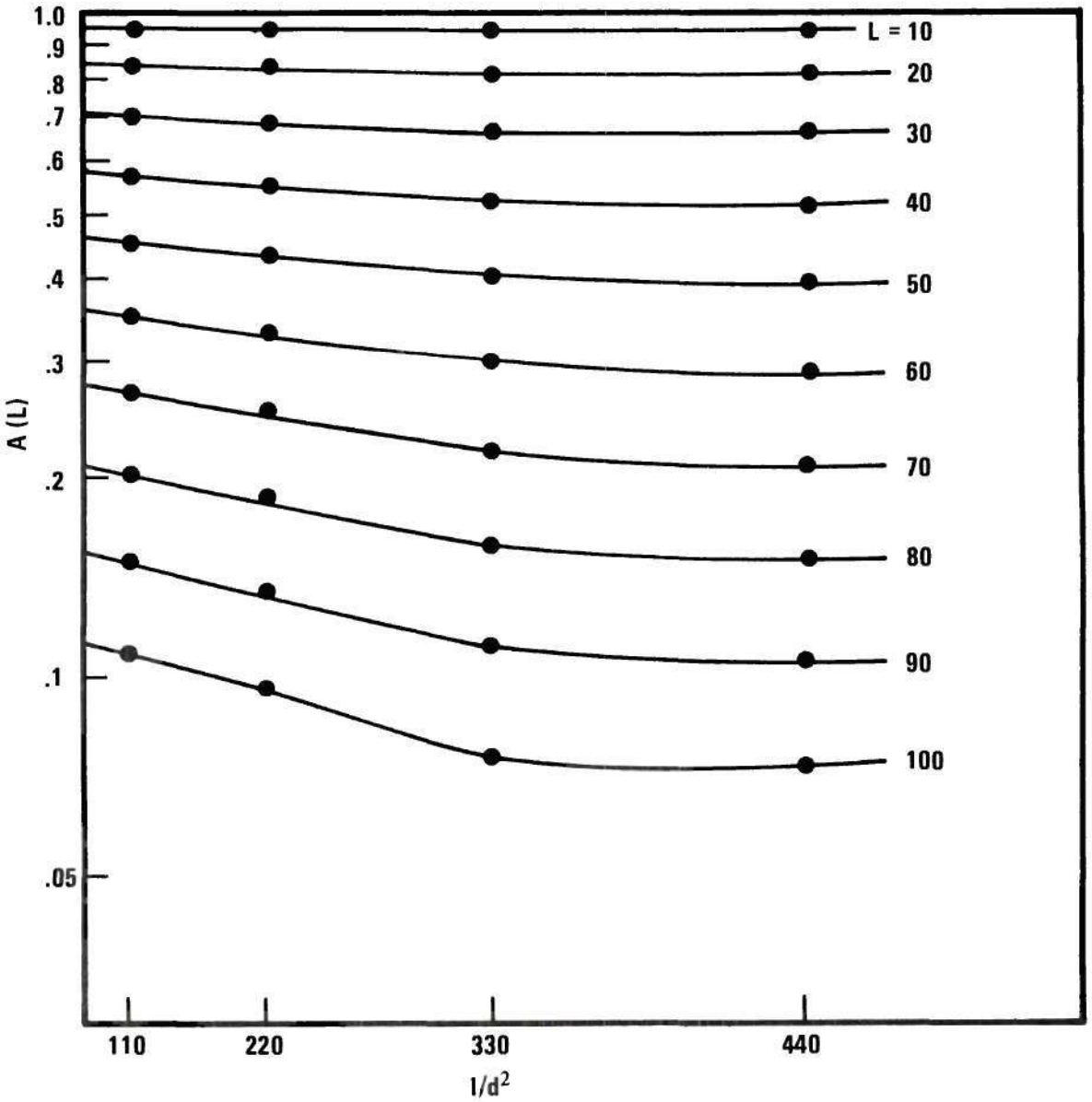

Figure 14. Fourier Coefficients of Various Orders of Reflection of a $(110)_T$ Plane for Different L Values.

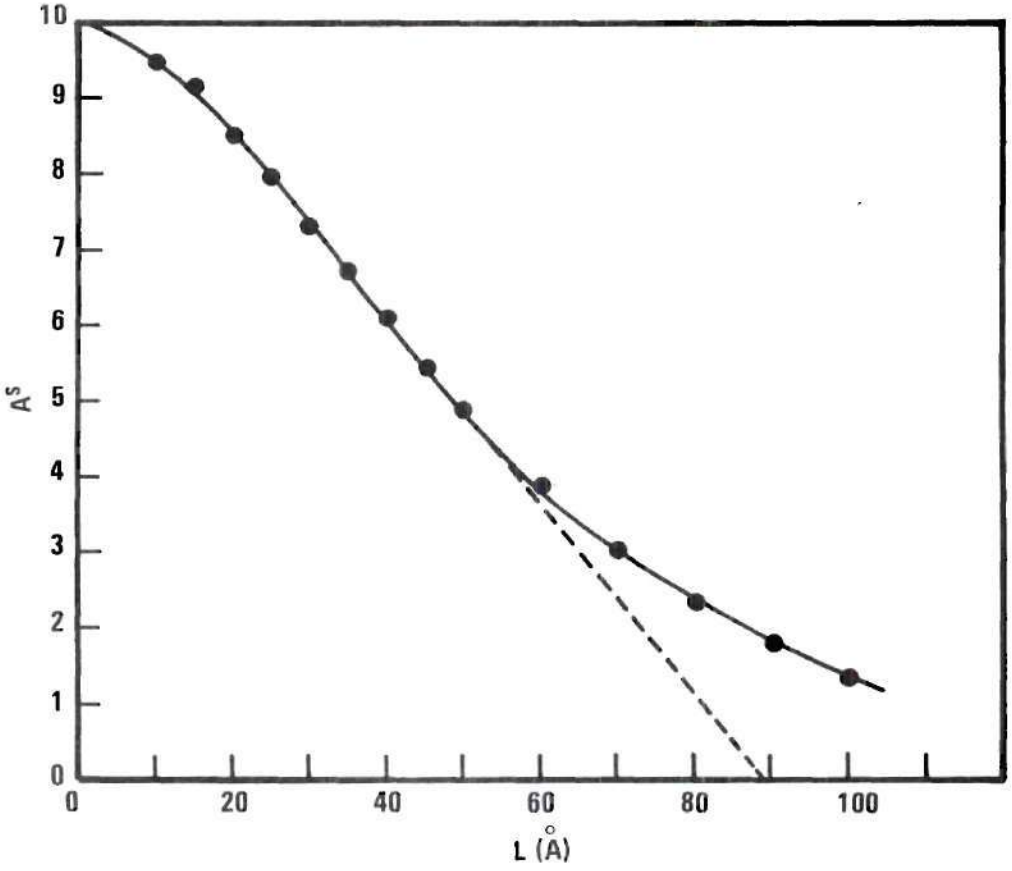

Figure 15. Plot of Fourier Size Coefficients Versus L.

The ratio,

$$\Delta L/L = (Z_{m'}' - Z_m)\, a_3' / (m' - m)\, a_3' = Z_n a_3' / n a_3' = \epsilon_L,$$

is a component of strain along the a_3' -direction with an undistorted distance $L = na_3'$, see Figure 16. Before taking the average over all the pairs of cells which are n cells apart, the value is squared so that the positive and negative strains will not cancel out. The squared value is then averaged over all the pairs n cells apart in the same column and then over all the columns in the domain and over all the domains in the sample. It is called the mean-square strain, and the value of its square-root is called root-mean-square (rms) strain, $\langle\, \epsilon_L^{\,2} \,\rangle^{\frac{1}{2}}$.

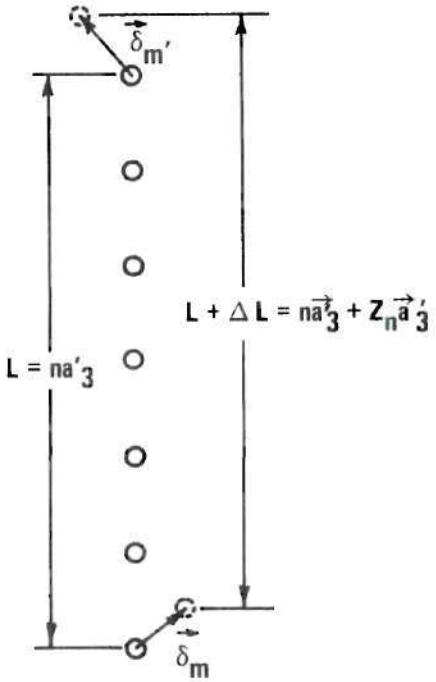

Figure 16. The Distortion of the Cells in a Column, the Circle Represents the Cell Center.

From the above definition of rms strain, one visualizes that it is a measurement of the average of the absolute distortion component in the

direction of the diffraction vector from all of the cells in the sample participating in the diffraction. This small cell displacement from the equilibrium position is due to crystalline defects, such as dislocations, faulting, interstitials, vacancies and coherent boundaries, and is dependent on the elastic constants of the crystal. If the displacement of the cells from their equilibrium position is only due to the presence of a random distribution of dislocations, the dislocation density may be estimated from the measured root-mean-square strain.[38]

$$\rho_{\epsilon} \simeq 12 \langle \epsilon^2_{50\text{Å}} \rangle / b^2 \qquad (A.12)$$

The effective particle size is determined from $N_3 a_3'$, where N_3 is the average number of cells per column. The continuity of the columns may be interrupted by dislocations, stacking faults, domain and grain boundaries. The effective particle size is then the total column length obtained from summing over all the broken column sections in the direction of the diffraction vector divided by the total number of these column sections. Hence the measured effective particle size in a crystallographic direction should be dependent on the orientation and distribution of dislocations and stacking faults. The dislocation density also can be estimated from the effective particle size. For a metal of low faulting probability and a random dislocation distribution, the effective particle size is about the average distance between dislocations,[39,40] and the dislocation density can be calculated from the effective particle size by

$$\rho_D \simeq \frac{1}{4 \langle D \rangle^2} \qquad (A.13)$$

The effective particle size is equal to the true particle size only if all the dislocations are in the subgrain boundaries and none in the subgrains themselves. This is never true in a real crystal. Hence it should be always kept in mind that the effective particle size measured by x-ray line broadening is not usually the same as the metallographic subgrain size, since it depends on the density, orientation and distribution of dislocations and stacking faults. Since the measured effective particle size is affected by the dislocation distribution much more than the measured rms, the square root of the ratio of ρ_ϵ to ρ_D is used as an indication of the dislocation distribution. A completely random distribution gives a ratio of unity.[38,41]

Determination of the Degree of Order

The integrated intensity of an x-ray reflection can be calculated from the equation,[1]

$$I_{hk\ell} = \text{Const.}\ (LP)\ P_{hk\ell}\ F^2_{hk\ell} \qquad (A.14)$$

where LP is the Lorentz-polarization factor, $P_{hk\ell}$ is the number of planes in the form $\{hk\ell\}$, and $F_{hk\ell}$ is the structure factor which involves a sum over all the atom positions in the unit cell.

$$F_{hk\ell} = \sum_{n=1}^{N} f_n e^{2\pi i(hx_n + ky_n + \ell z_n)} \qquad (A.15)$$

where N is the number of atoms in the unit cell, $hk\ell$ are the Miller indices, and x_n, y_n, z_n are the fractional coordinates of the n atom in the unit cell. This equation shows that the intensity of a possible reflection

depends on the relative disposition of the N atom in the unit cell and on their respective scattering powers f_n.

Each term in equation (A.15) can be considered to represent a wavelet with an amplitude f_n and a phase factor equal to $2\pi(hx_n + ky_n + \ell z_n)$ which expresses the path length for each scattered wavelet. Because of this phase factor, reflections from all planes which satisfy Braggs law are not always observed for randomly-oriented or pure materials. This is due to wavelet interference. For example, in bcc crystals all reflections from planes for which $(h + k + \ell)$ is odd will be extinguished due to interference effects. In ordered alloys, however, interference does not result in complete cancelation of the diffracted wave since the atomic scattering factors are different for different atomic species. Using β-brass as an example, the Cu atoms occupy the cube corners and the Zn atoms the cube centers. The general structure factor can be represented as $F = (f_{Cu} + f_{Zn})$ for $h + k + \ell$ = even (fundamental reflections) and $F = (f_{Cu} - f_{Zn})$ for $h + k + \ell$ = odd (superlattice reflections).

Using the definition of the long-range-order parameter given by Warren and described in the Chapter I, the structure factors for the superstructure reflections in partially ordered materials turns out to be proportional to S even for non-stoichiometric compositions. Consequently, the long-range-order parameter, S, can be obtained from a comparison of the integrated intensity of the fundamental and superlattice reflections. The formula used to calculate the structure factor of a partially ordered alloy becomes

$$F_{hk\ell} = \sum_{\alpha} (r_\alpha f_A + w_\alpha f_B)\, e^{2\pi i(hx_n + ky_n + \ell z_n)}$$

$$+ \sum_{\beta} (r_\beta f_B + w_\beta f_A)\, e^{2\pi i(hx_n + ky_n + \ell z_n)} \qquad (A.16)$$

where f_A, f_B are the atomic scattering factors of A and B kinds of atoms respectively. The summation is carried over all the α-sites and β-sites in the unit cell.

In the ordered Ni_4Mo, there are two molybdenum atoms and eight nickel atoms in the superlattice unit cell. The atomic positions are,[42] Mo: (000), ($\frac{1}{2}\frac{1}{2}\frac{1}{2}$), Ni: (2/5 1/5 0), (4/5 2/5 0), (1/10 3/10 $\frac{1}{2}$), (7/10 1/10 $\frac{1}{2}$), (9/10 7/10 $\frac{1}{2}$), (3/10 9/10 $\frac{1}{2}$), (1/5 3/5 0), (3/5 4/5 0). The structure factor of Ni_4Mo is evaluated by putting the atom positions into equation (A.16). The generalized structure factors are:

$F_{hk\ell} = 0$ for $h + k + \ell$ = odd,

$F_{nk\ell} = 5(X_B f_B + X_A f_A)$ for fundamental reflections which result from successive layers which have identical mixed packing with every fifth atom being Mo, where X_A, X_B are the sample composition in atom fractions,

$F_{hk\ell} = S(f_B - f_A)$ for superlattice reflections which result from layers of unmixed atoms with every fifth layers being Mo.

The long-range-order parameter, S, can then be determined by comparing the integrated intensity of a superstructure reflection with that of a fundamental reflection. As the low-order fundamental reflections are much stronger than the superlattice reflections, and their measured values more influenced by extinction effects, the weaker high-order fundamentals are compared with the strongest superlattice reflections. This minimizes errors due to extinction effects. It should be emphasized, however, that the value of S determined by this method is an average.

The degree of order within the crystal may not be homogeneous; it may be different in the domains and at the boundaries.

APPENDIX B

THE ALIGNMENT PROCEDURE FOR THE SINGLE CRYSTAL

The General Electric single crystal orienter which included a goniostat and a 7018A eucentric goniometer head was used for this experiment. Precise alignment was necessary in order to obtain accurate intensity data for Fourier analysis of the reflection profile. The criterion for this alignment was that the beam had to pass through the center of 2θ axis and also pass through the center of the receiving slit at $2\theta = 0.00°$ (see Figure 17).

The microscope on the detector arm was placed at approximately 100°, 2θ. Then a $\sim$0.002" diameter wire was put in the eucentric goniometer head at $\chi = 0.0°$. Using the goniometer head's angular adjustment and horizontal displacement screws, the wire was positioned so that it did not wobble during Φ rotation. Any wobble could be detected by viewing through the microscope.

After the wire was adjusted to remove the wobble, the microscope screws were loosened. The microscope was rotated and adjusted so that its vertical cross hair coincided with the wire when the wire was at $\chi = 0.0°$. Then the wire was rotated to $\chi = 90.0°$ and the microscope was adjusted so that the horizontal cross hair would coincide with the wire. Once this was accomplished, the screws which fasten the microscope to the detector arm were tightened. The microscope was then moved to exactly focus on the wire. After this focusing, the position of the microscope was marked on

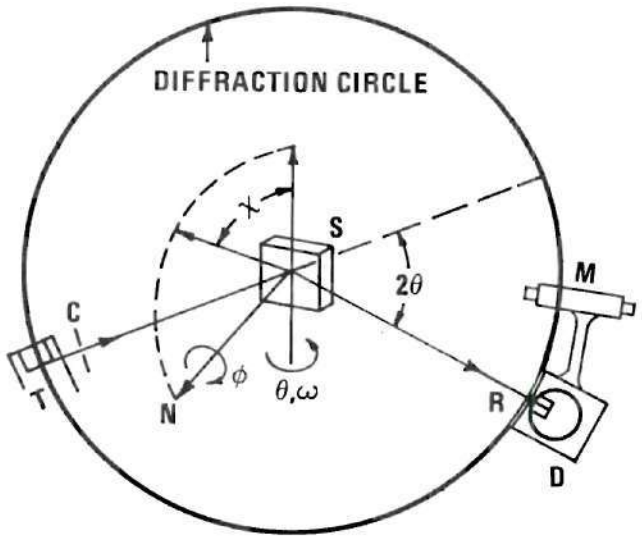

Figure 17. Schematic of
Diffractometer Geometry for Line Profile Measurements

the track. This was important for precise orientation of the sample.

The diffractometer was then moved to zero degree of 2θ. To protect the detector a lead stop was placed on its entrance. When the equipment was in correct alignment, the beam, the wire and the receiving slit were in the position so that the wire divided the beam symmetrically and an equal portion of the divided beam entered the receiving slit. This condition was easily checked with a small fluorescent screen placed behind the receiving slit. When the alignment was correct the rectangular image of the receiving slit was divided into two equal parts by the wire. This was necessary for the wire in both the vertical or horizontal positions ($\chi = 0.0°$ and $\chi = 90.0°$).

Vertical displacement of the beam was accomplished by the leveling screws of the diffractometer. Horizontal splitting of the receiving slit image by the wire when it is at $\chi = 0.0°$ was achieved by moving the goniometer about the source by adjustment of the take-off angle on diffractometer. The alignment was verified by obtaining equal intensity from a low angle reflection on both sides of 0.0° (2θ).

Since the single crystal orienter had been aligned with the diffractometer, the next step was to establish a simple method to search for the desired diffraction peak, and to obtain a corrected intensity distribution. A single crystal of LiF was chosen for this purpose because the sample surface is perfectly parallel to the (100) plane, which is the cleavage plane.

The diffractometer was rotated to 100.00°, 2θ position. The inclination angle χ was adjusted to zero. The LiF sample was placed horizontally on the top of the goniometer head. The sample position was

adjusted so that the microscope could focus on both sides of the crystal edge when Φ rotated 180 degrees. Then the arcs were adjusted so that all the edges of the crystal face were parallel to the horizontal line of the cross hair when the crystal rotated about the Φ axis. The microscope was then brought to the previous marked position. The microscope was then focused on the crystal surface. A focusing light was found necessarily to project on the crystal surface to see a clear focusing line. The height of the crystal was then adjusted so that the focusing line coincided with the horizontal cross hair of the microscope. The diffractometer was then rotated to 45.03 degrees (2θ), which is the Bragg angle for the (200) plane of the LiF crystal. Then χ was adjusted to 90 degrees. The (200) peak intensity could be detected in this arrangement (a slight adjustment of the angle χ and Φ was necessary to get the optimum intensity). ω was then adjusted so that the peak intensity was maximum and the position of ω was then marked. The diffractometer was rotated to 100.00 degrees (2θ). The microscope was adjusted back to focus on the crystal edge. The crystal was rotated through 180 degrees and was checked as to whether both the crystal edges were in focus at the same position; if not, the diffractometer (2θ) was adjusted so that the axis of the microscope was parallel to the crystal surface. The position of the diffractometer (2θ) was then marked. This was the reference position for later alignments.

When the real sample was used, the procedures were the same except that the previous marked positions for ω and 2θ were used. However, usually the sample surface edges were not very sharp, and the sample surface was not exactly parallel to the crystallographic plane being studied. As a result it was impossible to exactly align the sample this

way. Further alignment was obtained by slightly adjusting χ and Φ in order to pinpoint the peak maximum of the particular plane in question.

It was important to be sure that the x-ray beam passing through the confined slit would all fall on the sample surface especially at small 2θ value. To get an idea of the necessary surface size, the sample was replaced by an x-ray film and exposed for a required amount of time. The beam size was then adjusted to fulfill this requirement.

APPENDIX C

COMPUTER PROGRAM

A computer program was written in Fortran IV to transform a peak profile into a Fourier series. The coefficients of this series were used to calculate the particle size and root-mean-square strain. A flow chart of the program is shown in Figure 18.

Before computing the Fourier coefficients, the following corrections were made on the input intensity data: (i) subtraction of the background intensities, (ii) correction of Lorenz-polarization factor, (iii) calculation of the $K\alpha_1$ intensity component from the $K\alpha_1$ -$K\alpha_2$ doublet using the Rachinger method, (iv) conversion of the 2θ scale into $\sin\theta$ scale, (v) computation of the intensity maximum and/or centroid. The atomic scattering factors and temperature factor are, in principle, functions of 2θ for a same wave length, but were negligible for this experiment where only the peak broadening was of interest. The corrected intensity profile designated as $P''(2\theta)$ was then used to calculate the Fourier coefficients according to the following equations:

$$A_n = \int_{s-\frac{1}{2}}^{s+\frac{1}{2}} P''(h_3) \cos 2\pi n h_3 \, dh_3$$

$$B_n = \int_{s-\frac{1}{2}}^{s+\frac{1}{2}} P''(h_3) \sin 2\pi n h_3 \, dh_3$$

Here s represents a point in the reciprocal space corresponding to θ_0,

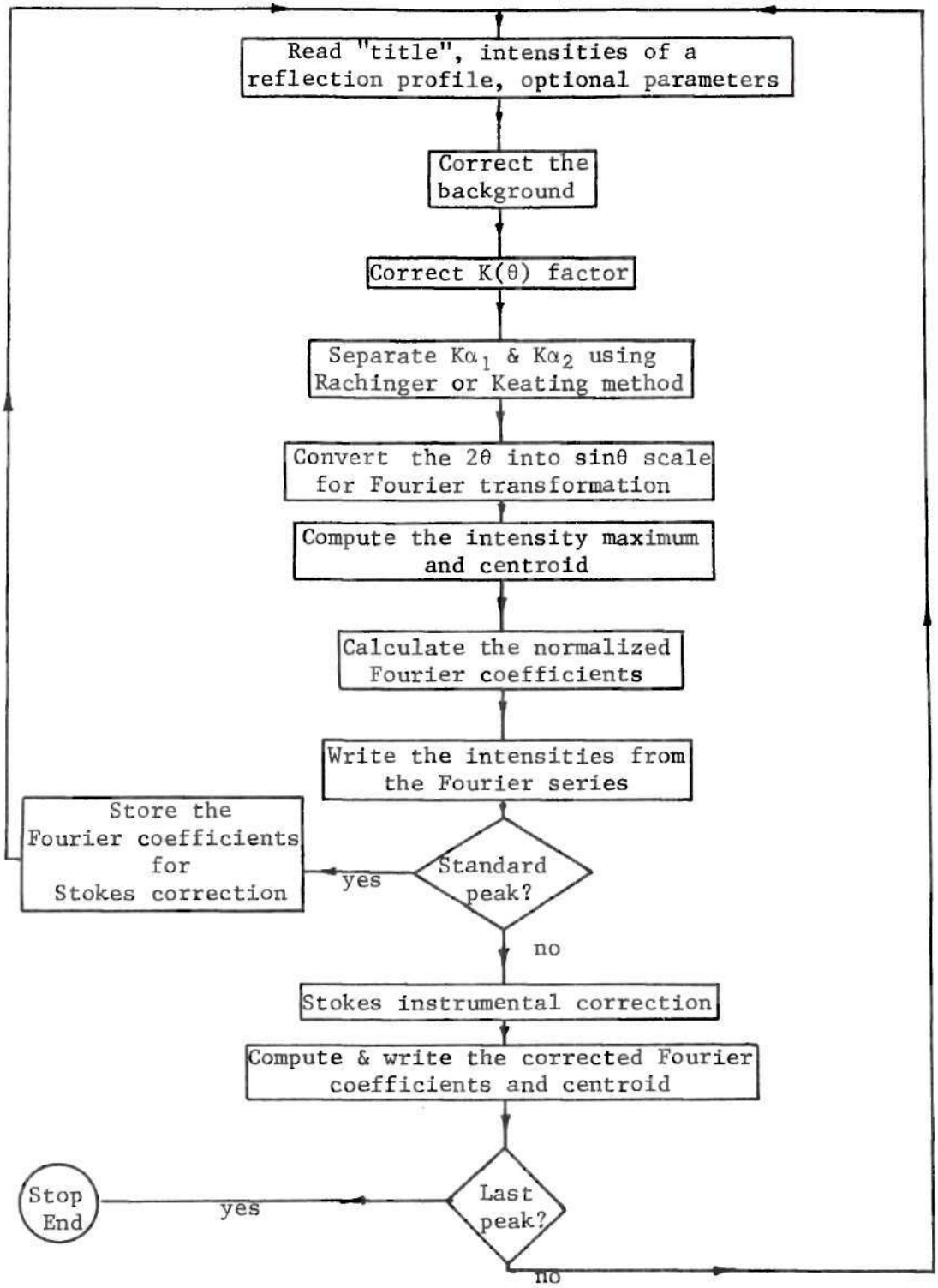

Figure 18. Flow Chart for the Computer Program.

the peak origin, and was the peak centroid in the present experiment.

The intensity data were taken in the 2θ-scale. These data were transformed into reciprocal space coordinates in order to carry out the integration of equations (C.1) and (C.2). The reciprocal space variable h_3 is related to the 2θ scale by

$$h_3 = (2a_3 \sin\theta)/\lambda \tag{C.3}$$

In order to carry out the integration numerically, a set of fictitious quantities a_3', s', h_3' and n' were introduced, so that equation (C.3) became

$$h_3' = (2a_3' \sin\theta)/\lambda \tag{C.4}$$

An interval form θ_1 to θ_2 was selected which was large enough to include all the observable intensity variations in the peak, and θ_0 was the computer-calculated peak origin for the transformation. Equation (C.4) may be written in terms of θ_1, θ_0 and θ_2 as

$$s-\tfrac{1}{2} = (2a_3'/\lambda) \sin\theta_1 \tag{C.5}$$

$$s = (2a_3'/\lambda) \sin\theta_0 \tag{C.6}$$

$$s+\tfrac{1}{2} = (2a_3'/\lambda) \sin\theta_2 \tag{C.7}$$

From equations (C.5) and (C.6) the following equation can be obtained

$$\tfrac{1}{2} = (2a_3'/\lambda) (\sin\theta_0 - \sin\theta_1) \tag{C.8}$$

which defines the value of the fictitious a_3'. The selection of θ_2 was done before the calculation of the θ_0, hence the corrected θ_2 value which corresponded to the corrected origin, θ_0, and a_3' had to be recalculated to satisfy the following equation,

$$\tfrac{1}{2} = (2a_3'/\lambda)\ (\sin\theta_2 - \sin\theta_0) \qquad (C.9)$$

The corrected θ_2 value was truncated by computer methods from the input intensity data, and the intensity data beyond θ_2 were disregarded in the computation. Hence, when choosing the interval, θ_1 to θ_2, it was required that $(\sin\theta_2 - \sin\theta_0') \geq (\sin\theta_0' - \sin\theta_1)$, where θ_0' was the visually estimated peak origin. The intensity data at θ_1 and θ_2 were used to correct for background intensity by assuming a linear background intensity distribution for a peak.

The numerical solution of equations (C.1) and (C.2) were carried out by dividing the h_3 scale into equal segments. Since a_3' and λ are constants for a particular peak, equal h_3 segments according to equation (C.4) result in equal values of $\sin\theta$ scale. Let the infinitesimal segment be $\Delta h_3'$, then

$$\Delta h_3' = (2a_3'\ \Delta\sin\theta)/\lambda$$

where $\Delta\sin\theta = (\sin\theta_0 - \sin\theta_1)/p$, p is an integer about 50 per degree for $(\theta_0 - \theta_1)$. The numerical solutions of equations (C.1) and (C.2) then become

$$A_n = \sum_{i=0}^{p} P''[(h_3')_i] \cos 2\pi n'(h_3')_i\ (\Delta h_3')$$

and

$$B_n = \sum_{i=0}^{P} P''[(h_3')_i] \sin 2\pi n'(h_3')_i \ (\Delta h_3')$$

The summations were carried out by "do loop" of the program. The Fourier coefficients A_n and B_n were calculated from n' = 0 to a desired value. The real distance along the direction perpendicular to the reflecting planes was defined as L = n'a'.

All the Fourier coefficients calculated from each of the peaks were then normalized so that the instrumental broadening of the cold worked peaks could be corrected by Stokes' method.[36] The computer program could analyze as many peaks as desired within one run time.

The computer program is on file on tape at the Rich Computer Center, Georgia Institute of Technology.

BIBLIOGRAPHY*

1. B. E. Warren, "X-ray Diffraction," Addison-Wesley Publ. Co., Reading, Mass. (1969).

2. J. W. Christian, "The Theory of Transformations in Metals and Alloys," Pergamon Press, Oxford (1965).

3. Von W. S. Gorsky, Phys. Z. Sowjetunion 8, 443 (1935).

4. G. H. Vineyard, Phys. Rev. 102, 981 (1956).

5. P. S. Rudman, Paper Presented at AIME Annual Meeting, Feb. 1964, Dept. of Physics Technion Israel Inst. Haifa, Israel.

6. G. E. Poquette and D. E. Mikkola, Trans. AIME 245, 743 (1969).

7. T. Muto and Y. Takagi, Solid State Phys. 1, 194, Academic Press, New York (1955).

8. L. Guttman, Solid State Phys. 3, 145, Academic Press, New York (1956).

9. N. S. Stoloff and R. G. Davies, "Progress in Materials Science," edited by Bruce Chalmers, 13, Pergamon Press, New York (1966).

10. R. W. Cahn, "Local Atomic Arrangements Studied by X-ray Diffraction," edited by J. B. Cohen and J. Hilliard, Gordon and Breach, New York (1967).

11. P. A. Flinn, Trans, AIME 218, 145 (1960).

12. A. H. Cottrell, "Relation of Properties of Microstructure," Amer. Soc. Metals, Cleveland (1955).

13. B. H. Kear, Acta Met. 12, 555 (1964).

14. V. S. Arumachalam and R. W. Cahn, J. Mater. Sci. 2, 160 (1967).

15. M. Hirabayoshi and S. Ogawa, J. Phys. Soc. Japan 11, 907 (1956).

16. S. Kohara and G. C. Kuczynski, Acta Met. 4, 221 (1956).

17. E. Ruedl, P. Delavignette, and S. Amelinckx, Phys. Stat, Sol. 28, 305 (1968).

*Abbreviations found herein follow the form in Access, 1969.

18. B. Chakravarti, E. A. Starke, Jr., and B. G. LeFevre, J. of Mater. Sci. 5, 394 (1970).

19. Toshio Saburi, Kimio Komatsu, and Soji Nenno, Phil. Mag. 20, 1091 (1969).

20. Toshio Saburi, (Private Communication).

21. Paul R. Okamoto, Ph.D. Thesis, University of Cal. Berkeley, March, 1970.

22. J. E. Spruiell, Ph.D. Thesis, Univ. of Tennessee (1963).

23. D. E. Mikkola and J. B. Cohen, "Local Atomic Arrangement Studied by X-ray Diffraction," edited by J. B. Cohen and J. E. Hilliard, Gordon and Breach, New York (1967).

24. R. A. Buchanan, J. J. Wert, and S. G. Cupschalk, Trans. AIME 245, 11 (1969).

25. E. A. Starke, Jr., J. C. Ogle, and C. J. Sparks, Jr., Advance in X-ray Analysis 12, 372 (1969).

26. S. L. Mannan and V. S. Arunachalam, Scripta Metallurgica 3, 597 (1969).

27. J. G. Byrne, "Recovery Recrystallization and Grain Growth," MacMillan, New York (1965).

28. R. L. Fullman, "Metal Interfaces," American Society for Metals, Cleveland, Ohio (1952).

29. A. T. English, Trans. AIME 236, 14 (1966).

30. R. G. Davies and N. S. Stoloff, Trans. AIME 230, 390 (1964).

31. Paul Gordon and T. A. El-Bassyouni, Trans. AIME 133, 391 (1965).

32. L. M. Brown and G. R. Woolhouse, Phil. Mag. 21, 329 (1970).

33. B. E. Warren, "Progress in Metal Physics," edited by Bruce Chalmers, 8, Pergamon Press, New York (1959).

34. F. W. Ling and E. A. Starke, Jr., J. Appl. Cryst. (in press).

35. "Metals Handbook," Volume 1, American Society of Metals, Metals Park, Ohio (1961).

36. A. R. Stokes, Proceedings of Physical Society 61, 382 (1948).

37. F. Bertaut, C. R. Acad. Sci. Paris 228, 492 (1948).

38. K. Williamson and R. E. Smallman, Phil. Mag. 1, 34 (1956).

39. R. W. Hinton, L. H. Schwartz, and J. B. Cohen, J. Electro Chem. Soc. 110, 103 (1963).

40. K. P. Ryaboshapka and L. V. Tichonov, Fiz, Metal Metalloved 12, 1 (1961).

41. R. E. Trahocco and R. W. Heckel, Trans. AIME 242, 1945 (1968).

42. D. Harker, J. Chem. Phys. 12, 315 (1944).

VITA

Fu-Wen Ling, son of Mr. & Mrs. Chao-Kao Ling, was born in Tainan, Taiwan on November 28, 1937. He was educated in the Pei-Moon High School, Tainan, Taiwan for three years, then attended Tainan Industrial Vocational School, Tainan, Taiwan in September, 1953 and was graduated in July, 1956. He entered Cheng-Kung University, Tainan, Taiwan in September, 1957 and majored in Mechanical Engineering. In June, 1961 he received the Bachelor of Science degree.

After one year service in the Chinese Navy he worked in the Taiwan Sugar Corporation, Kaushoung, Taiwan for one year. From September, 1963 to August, 1965 he was employed as a full time teaching assistant in the Department of Mechanical Engineering, Cheng-Kung University. In September, 1965 he came to the United States and entered Auburn University, Auburn Alabama, where he received a Master of Science in Mechanical Engineering in August, 1967, and continued as a two-thirds time graduate research and teaching assistant until December, 1968. In January, 1969, he entered the Graduate Division of the Georgia Institute of Technology.

He married the former Elena Mei-Fei Huang of Tainan, Taiwan in June, 1970.